JCB Journal of Cell Biology

ARTICLE

Border cell polarity and collective migration require the spliceosome component Cactin

Guangxia Miao[1], Li Guo[1], and Denise J. Montell[1]

Border cells are an in vivo model for collective cell migration. Here, we identify the gene *cactin* as essential for border cell cluster organization, delamination, and migration. In Cactin-depleted cells, the apical proteins aPKC and Crumbs (Crb) become abnormally concentrated, and overall cluster polarity is lost. Apically tethering excess aPKC is sufficient to cause delamination defects, and relocalizing apical aPKC partially rescues delamination. Cactin is conserved from yeast to humans and has been implicated in diverse processes. In border cells, Cactin's evolutionarily conserved spliceosome function is required. Whole transcriptome analysis revealed alterations in isoform expression in Cactin-depleted cells. Mutations in two affected genes, Sec23 and Sec24CD, which traffic Crb to the apical cell surface, partially rescue border cell cluster organization and migration. Overexpression of Rab5 or Rab11, which promote Crb and aPKC recycling, similarly rescues. Thus, a general splicing factor is specifically required for coordination of cluster polarity and migration, and migrating border cells are particularly sensitive to splicing and cell polarity disruptions.

Introduction

Embryonic development requires extensive cell migrations (Scarpa and Mayor, 2016; Yang et al., 2020). Movements of tumor cells, endothelial cells, fibroblasts, and immune cells also contribute to tumor metastasis (Stuelten et al., 2018). Such movements can be collective and involve multiple cell types. For example, cancer-associated fibroblasts lead migrating tumor cell collectives (Labernadie et al., 2017), macrophages promote breast cancer dissemination (Goswami et al., 2005), and in at least some types of cancer, cells circulating collectively are more effective at seeding distant metastases than single cells (Aceto et al., 2014; Au et al., 2016; Cheung et al., 2016).

Border cells in the *Drosophila* ovary serve as a model for collective, cooperative cell migration that is amenable to genetic screening and live imaging (Montell et al., 2012). Border cells are a group of 6–10 cells derived from the follicular epithelium, which surrounds the developing germline during oogenesis in *Drosophila* (Fig. 1, A–D). A special pair of follicle cells named polar cells develops at each end of the egg chamber. These polar cells secrete a cytokine that activates Janus kinase/signal transducer and activator of transcription (JAK/STAT) signaling and motility in the neighboring cells (Silver and Montell, 2001), which then begin to extend and retract dynamic protrusions in between the adjacent germ cells, called nurse cells. Eventually the cells delaminate from the epithelium and squeeze between the 15 nurse cells, traveling ∼150 µm until they reach the anterior border of the oocyte. When they arrive, the border cells attach to the oocyte and inwardly migrating follicle cells, called centripetal cells, forming a continuous epithelium in a process termed neolamination (Miao et al., 2020). Border cells and centripetal cells construct an eggshell structure essential for sperm entry (Montell et al., 1992) and secrete a critical patterning signal (Savant-Bhonsale and Montell, 1993). Thus, if border cell migration fails, females are sterile.

While much is known concerning the chemical, physical, mechanical, and adhesive factors that steer the border cells (Montell et al., 2012; Dai et al., 2020) and the cytoskeletal determinants of their morphology (Chen et al., 2020; Majumder et al., 2012; Aranjuez et al., 2016; Murphy and Montell, 1996), less is known about the mechanisms that govern their initial delamination from the follicular epithelium and the coordination of individual cell polarization, morphology, and behavior. Border cells undergo morphological hallmarks of a partial epithelial to mesenchymal transition (EMT), though they do not appear to depend upon classic EMT transcription factors. Instead, JAK/STAT activity is necessary and sufficient to confer migratory behavior (Silver and Montell, 2001). Multiple additional transcription factors feed back to distinguish migratory from nonmigratory cell fates (Jang et al., 2009; Berez et al., 2020; Monahan and Starz-Gaiano, 2013; Manning et al., 2017; Starz-Gaiano et al., 2008).

[1]Molecular, Cellular, and Developmental Biology Department, University of California, Santa Barbara, Santa Barbara, CA.

Correspondence to Denise Montell: dmontell@ucsb.edu; Guangxia Miao: miaoguangxia@gmail.com.

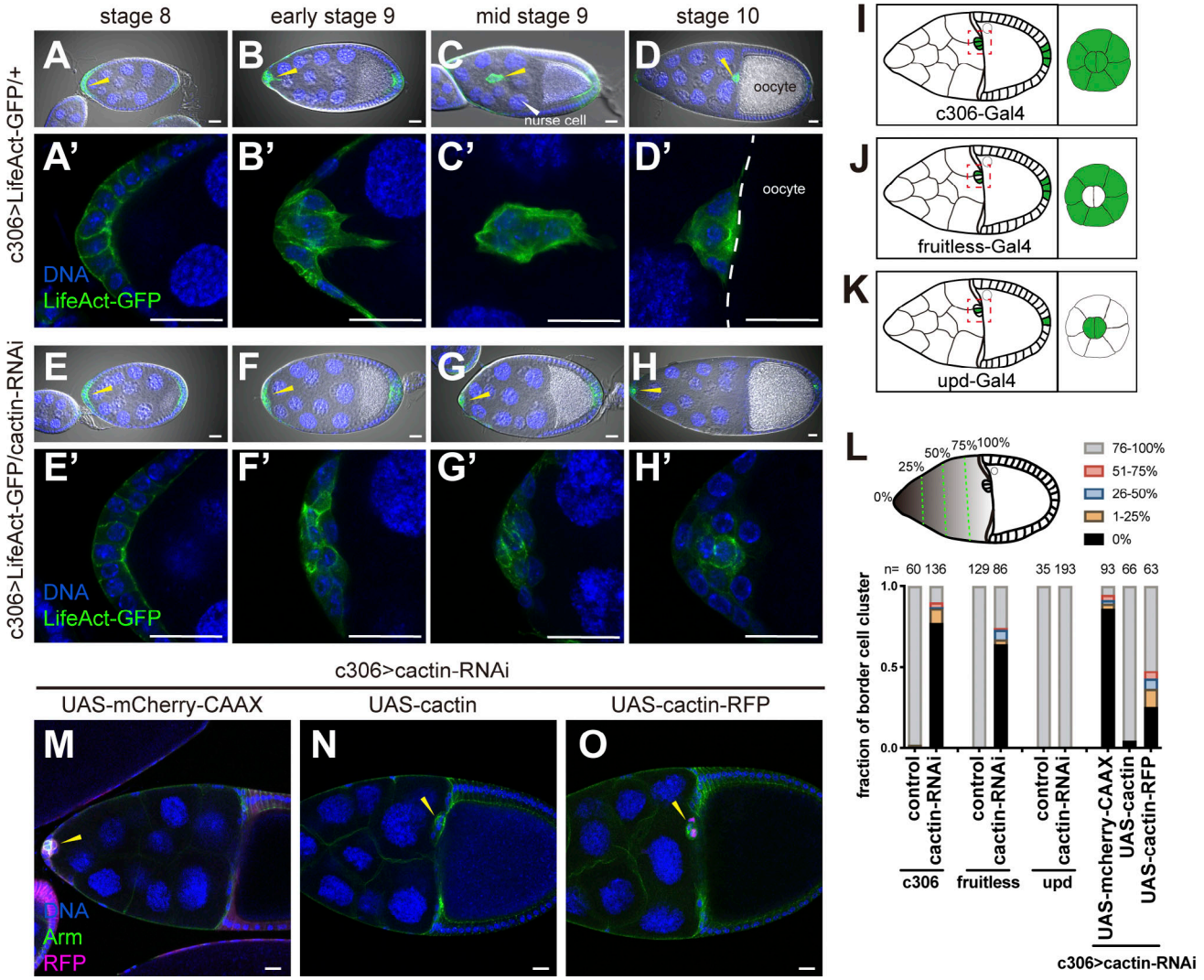

Figure 1. **Cactin is required for border cell delamination. (A–D)** Confocal micrographs of c306-Gal4, UAS-LifeAct-GFP/+ egg chambers of the indicated stages. differential interference contrast imaging is shown in grayscale, DNA in blue, and GFP in green. **(A′–D′)** High-magnification images of the GFP channels for A–D. **(E–H)** Images of similar stage egg chambers from c306-Gal4, UAS-LifeAct-GFP/*cactin*-RNAi females, labeled as in A–D. **(E′–H′)** High magnification images of E–H. **(I–K)** Schematic of the expression patterns of (I) c306-Gal4, (J) *fruitless*-Gal4, and (K) *upd*-Gal4. **(L)** Quantification of delamination defects in stage 10 egg chambers. Histogram shows the distribution of border cell clusters along the migration path in stage 10. **(M–O)** Confocal images of stage 10 egg chambers with c306-Gal4 driving UAS-*cactin*-RNAi together with (M) UAS-mCherry-CAAX, (N) UAS-*cactin*, or (O) UAS-*cactin*::RFP in magenta. Yellow arrowheads indicate the border cell clusters. Scale bars, 20 µm.

Here, we report that RNAi knockdown of the gene *cactin* causes severe defects in border cell delamination. In *cactin*-RNAi follicle cells, the apical proteins aPKC and Crumbs (Crb) become highly concentrated apically. Individual Cactin-depleted border cells are polarized and mobile, but protrusion, cluster polarity, organization, and migration are severely diminished. Reduction of aPKC ameliorates the defects, and tethering excess aPKC to apical membranes is sufficient to impair delamination. Cactin was first identified in *Drosophila* as a protein that binds and inhibits Cactus, which is an inhibitor of Dorsal, the fly NF-κB homolog (Lin et al., 2000). In *Caenorhabditis elegans*, the Cactin homolog CACN-1 inhibits the mig-2/Rac pathway to regulate distal tip cell migration (Tannoury et al., 2010), and human Cactin is a component of the spliceosome complex C. Human Cactin interacts with spliceosome-associated factors DHX8 and SRRM2 to ensure efficient pre-RNA splicing and sister chromatid cohesion (Zanini et al., 2017). We found that the Cactin spliceosome function is required for border cell cluster polarization and coordination of individual cell behaviors to produce coherent, collective movement. We report global changes in mRNA isoform expression in Cactin knockdown cells. Mutations in two affected genes, Sec23 and Sec24CD, which promote Crb trafficking to the apical domain, dominantly suppress *cactin*-RNAi phenotypes. We conclude that the general splicing factor Cactin is required for specific features of coordinating collective cell polarity and migration. Moreover, border cells are particularly vulnerable to polarity disruptions, possibly due to their loss of cues from the basement membrane and neighboring cells as they delaminate from the follicular epithelium. These findings may shed light on how mutations affecting general factors can

have cell-type specific effects, a phenomenon observed in numerous human diseases.

Results

Cactin is required for border cell delamination

To identify mechanisms of border cell delamination, we performed an RNAi screen of genes previously identified by mRNA expression profiling as enriched in border cells (Wang et al., 2006). Using c306-Gal4, which is expressed in border cells before and during migration (Fig. 1, A–D′), three UAS-*cactin*-RNAi lines showed strong delamination defects compared to controls (Fig. 1, E–H′; and Fig. S1, A–D). In control egg chambers, border cells are specified in stage 8 (Fig. 1, A and A′), then round up and extend and retract protrusions (Fig. 1, B and B′), migrate in between the nurse cells during stage 9 (Fig. 1, C and C′), and arrive at the oocyte by stage 10 (Fig. 1, D and D′). In Cactin-depleted border cells, however, no major forward-directed protrusions were observed (Fig. 1, E–G′). By stage 10, most *cactin*-RNAi-expressing clusters had failed to delaminate and remained at the egg chamber anterior (Fig. 1, H and H′).

Next, we asked which cell types required Cactin. The c306-Gal4 driver is expressed in both the outer, migratory border cells and the inner, nonmigratory polar cells, which the cluster carries to the oocyte (Fig. 1 I). To distinguish whether Cactin is required in border cells and/or polar cells, we expressed *cactin*-RNAi with *fruitless*-Gal4 (Fig. 1 J), which expresses in outer, migratory cells but not polar cells, and *upd*-Gal4 (Fig. 1 L), a polar cell driver. *Fruitless*-Gal4 caused a similar delamination defect as c306-Gal4 (Fig. 1 L), while *upd*-gal4 did not (Fig. 1 L). These results show that Cactin is required in migratory border cells.

We then generated UAS-*cactin* and UAS-*cactin*::RFP transgenic lines. Both UAS-*cactin* and UAS-*cactin*::RFP rescued *cactin*-RNAi delamination defects (Fig. 1, L–O). UAS-*cactin* fully rescued the delamination defect, while UAS-*cactin*::RFP reduced the incidence of delamination defects from 90% to ∼25% (Fig. 1 L), suggesting that RFP slightly impaired Cactin function. The rescue was not a consequence of titrating the Gal4 because the addition of UAS-mCherry-CAAX did not provide any rescue. Cactin::RFP protein localized predominantly to nuclei (Fig. 1 O; and Fig. S1, E and E′) and was substantially reduced in the presence of *cactin*-RNAi, confirming the effectiveness of the RNAi (Fig. S1, F–G). We conclude that Cactin is a predominantly nuclear protein required in migratory border cells during the delamination process.

Cactin functions independently of JAK/STAT or Toll signaling pathways in border cells

In stage 8, the polar cells secrete Upd, which activates STAT in neighboring cells (Fig. S2, A and A′) to specify them as migratory border cells. Fewer border cells form when JAK/STAT is reduced, and those that do form exhibit profound delamination and migration defects (Silver and Montell, 2001). To test whether Cactin knockdown might cause delamination defects by compromising JAK/STAT signaling, we combined the 10XSTAT-GFP activity reporter (Bach et al., 2007) with *cactin*-RNAi. We then measured GFP intensity in anterior follicle cells adjacent to the polar cells of stage 8 egg chambers (Fig. S2, A–B′). 10XSTAT-GFP intensity was ∼17% lower in *cactin*-RNAi–expressing cells (Fig. S2 C). This effect cannot explain the strong delamination defect caused by *cactin*-RNAi because a 50% reduction in STAT causes incomplete migration in only 10% of egg chambers and no delamination defect (Silver et al., 2005). Further, because JAK/STAT signaling alters border cell specification, border cell numbers are reduced when STAT activity is significantly impaired (Silver and Montell, 2001). We found no meaningful difference in border cell number between controls (3.9 ± 0.6, n = 9) and *cactin*-RNAi (3.5 ± 1.3, n = 10). We conclude that Cactin does not affect border cell delamination through the JAK/STAT pathway.

In *Drosophila*, Cactin was first identified as a Cactus binding protein, and Cactin overexpression enhanced *cactus* mutant phenotypes, which suggests Cactin is an inhibitor of Cactus (Lin et al., 2000). However, overexpression of Cactus did not cause a border cell delamination defect (Fig. S2, D–E′), and the Cactus protein level was unchanged in *cactin*-RNAi-expressing cells (Fig. S2, F and F′). Cactus is the fly ortholog of IkB, an inhibitor of NF-κB signaling. Thus, Cactin promotes NF-κB activity at least in some contexts. In *Drosophila*, Cactus plays a central role in Toll receptor signaling, which is required for dorsal/ventral patterning and the immune response (Valanne et al., 2011). To further test whether Cactin is related to Cactus in border cells, we performed an RNAi screen for components of the *Drosophila* Toll signaling pathway. We found that no RNAi line targeting the ligand Spätzle, the receptor Toll, the kinase Pelle, or myd88 caused a border cell delamination defect (Fig. S2 G). The only exceptions were two RNAi lines targeting the fly NF-κB homolog Dorsal (Fig. S2 G). By immunostaining, Dorsal is expressed in stalk and polar cells, but not detectably in border cells (Fig. S2, H–I′). Dorsal accumulates in the cytoplasm whereas it must translocate to the nucleus to function as a transcription factor. Dorsal expression and localization were unchanged in *cactin*-RNAi–expressing cells compared to control (Fig. S2, I–K′). Although it seems that Dorsal contributes to border cell migration perhaps by functioning in polar cells, together these results suggest Cactin function in border cells is independent of the Toll signaling pathway.

Cactin is required for border cell cluster polarization

To determine how border cell delamination is affected by *cactin*-RNAi, we carried out high-resolution fixed and live imaging to monitor border cell organization. In control egg chambers, four to eight migratory cells surround and carry two polar cells. The migratory cells round up and one or two cells extend a protrusion toward the oocyte. Eventually, one cell takes the lead while the other cells retract their protrusions (Fig. 2, A and B). Prior to migration, border cell and polar cell apical surfaces contact the germline, lateral surfaces adhere to each other, and basal surfaces adhere to the basement membrane that surrounds the egg chamber. As the cluster delaminates, protrusions extend from lateral surfaces and the cells retain a shared apicobasal polarization (Niewiadomska et al., 1999; Pinheiro and Montell, 2004; Wang et al., 2018). Additionally, as the cluster pulls away from the basement membrane and anterior follicle cells, it rotates

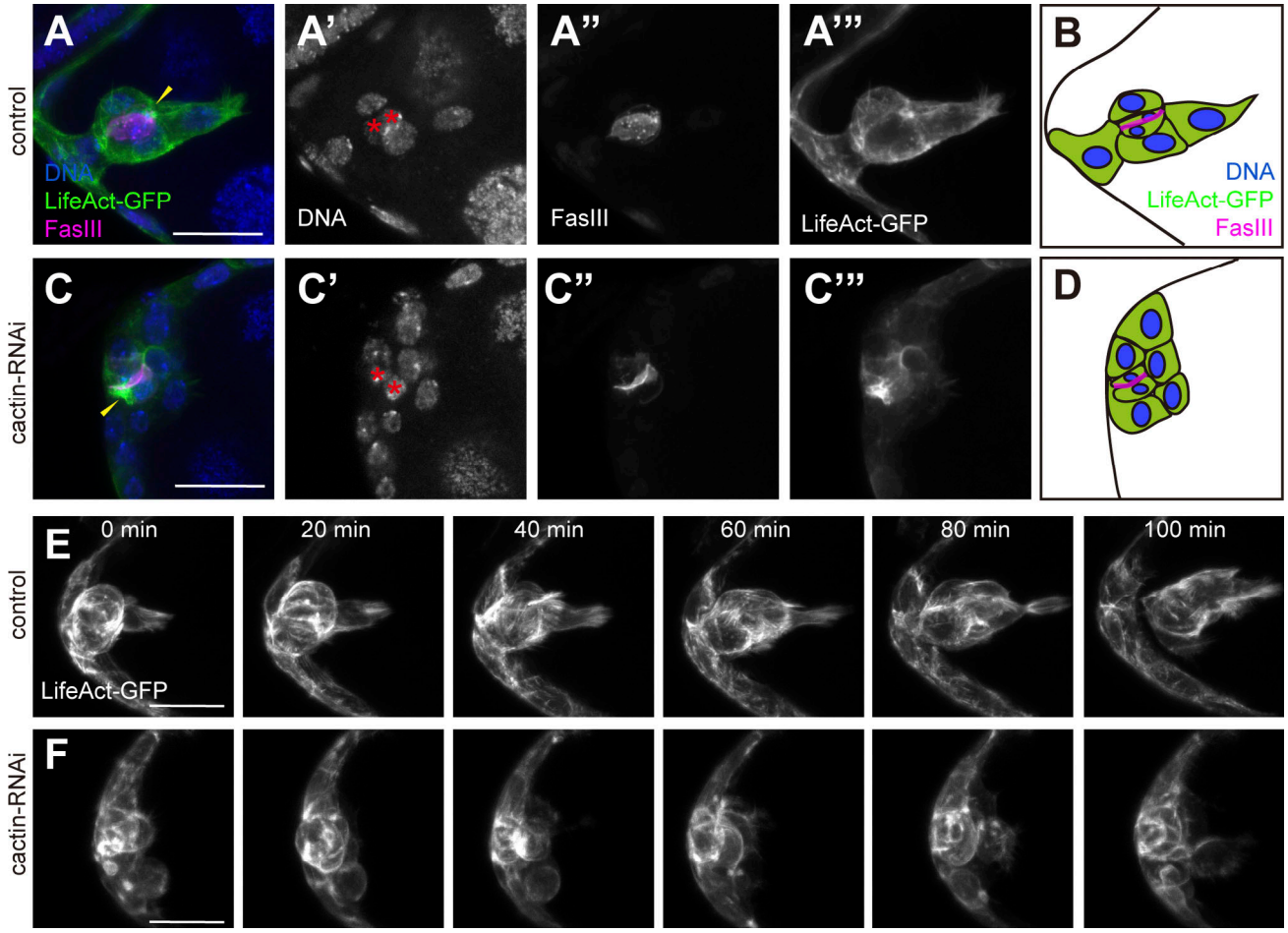

Figure 2. **Cactin is required for protrusion and border cell cluster polarization. (A and C)** Images of anti-FasIII staining early stage 9 egg chambers with c306-Gal4 driving UAS-LifeAct-GFP together with (A) control (crossed to *w1118*) or (C) UAS-*cactin*-RNAi. Yellow arrowheads indicate the apical junctions in the border cell cluster. Red asterisks mark the polar cells. Note that FasIII stained the interface between two polar cells. **(A′–A‴ and C′–C‴)** Images show the single channels in A and C. **(B and D)** Schematic of border cell organization in A and C. To avoid confusion, the angle of the two polar cell interfaces was adjusted in B. **(E and F)** Snapshots of time-lapse videos of c306-Gal4 driving UAS-LifeAct-GFP together with (E) control (cross to *w1118*) or (F) UAS-*cactin*-RNAi. Scale bars, 20 µm.

~90° so that the apical surface ends up roughly orthogonal to the direction of migration (Fig. 2, A and B).

In Cactin-depleted clusters, no cell took the lead, no large protrusion was observed (Fig. 2, C and D), and the cluster frequently failed to detach (Fig. 2, C and D). Live imaging revealed that, in contrast to controls (Fig. 2 E and Video 1), even though individual border cells were highly mobile, the movements of individual *cactin*-RNAi–expressing cells were not coordinated, so the clusters failed to advance (Fig. 2 F and Video 1). Furthermore, the apical polar cell surfaces were randomly oriented, sometimes even toward the anterior tip of the egg chamber, opposite from the direction of migration (Fig. 2, C and D), which was never seen in controls. The fixed and live imaging data suggest that depletion of Cactin disrupts protrusion and coordination of individual cell behaviors.

In control egg chambers, the follicle cells invariably form a monolayer, which covers the germline (Fig. 3, A–B‴). However, in 20% of *cactin*-RNAi–expressing egg chambers (27/136 egg chambers), follicle cells formed more than one layer within the c306-Gal4 expression domain at the posterior of the egg chamber (Fig. 3, C–D‴), which is characteristic of disrupted apicobasal polarity (Cox et al., 2001). So, we generated *cactin*-RNAi clones in the outer follicle cells and stained for aPKC, an apical marker. Relative to control clones (Fig. 3, E and E′), aPKC expression was increased apically in *cactin*-RNAi–expressing cells (Fig. 3, F and F′). In the most extreme cases, Cactin knockdown cells exhibited an approximately twofold increase in apical aPKC without significantly affecting overall aPKC levels (Fig. 3, E–I). These cells also exhibited apical constriction, which resulted in apical concentration of Armadillo (Arm; Fig. 3, G–H′).

Even in the absence of apical constriction, aPKC was 1.4-fold more concentrated at the apical surfaces of Cactin-knockdown cells compared to control cells (Fig. 3, J–L), suggesting that the excess aPKC was not simply a consequence of apical constriction. Neither myosin (Sqh::mCherry; Fig. 3, J‴, K‴, and L) nor Arm (Fig. S3, A–C) was concentrated at apical junctions in the unconstricted cells. These results suggest that Cactin normally prevents excess aPKC accumulation at apical epithelial cell surfaces.

We then examined aPKC localization in border cells. Control border cell clusters retain coordinated apicobasal polarity during

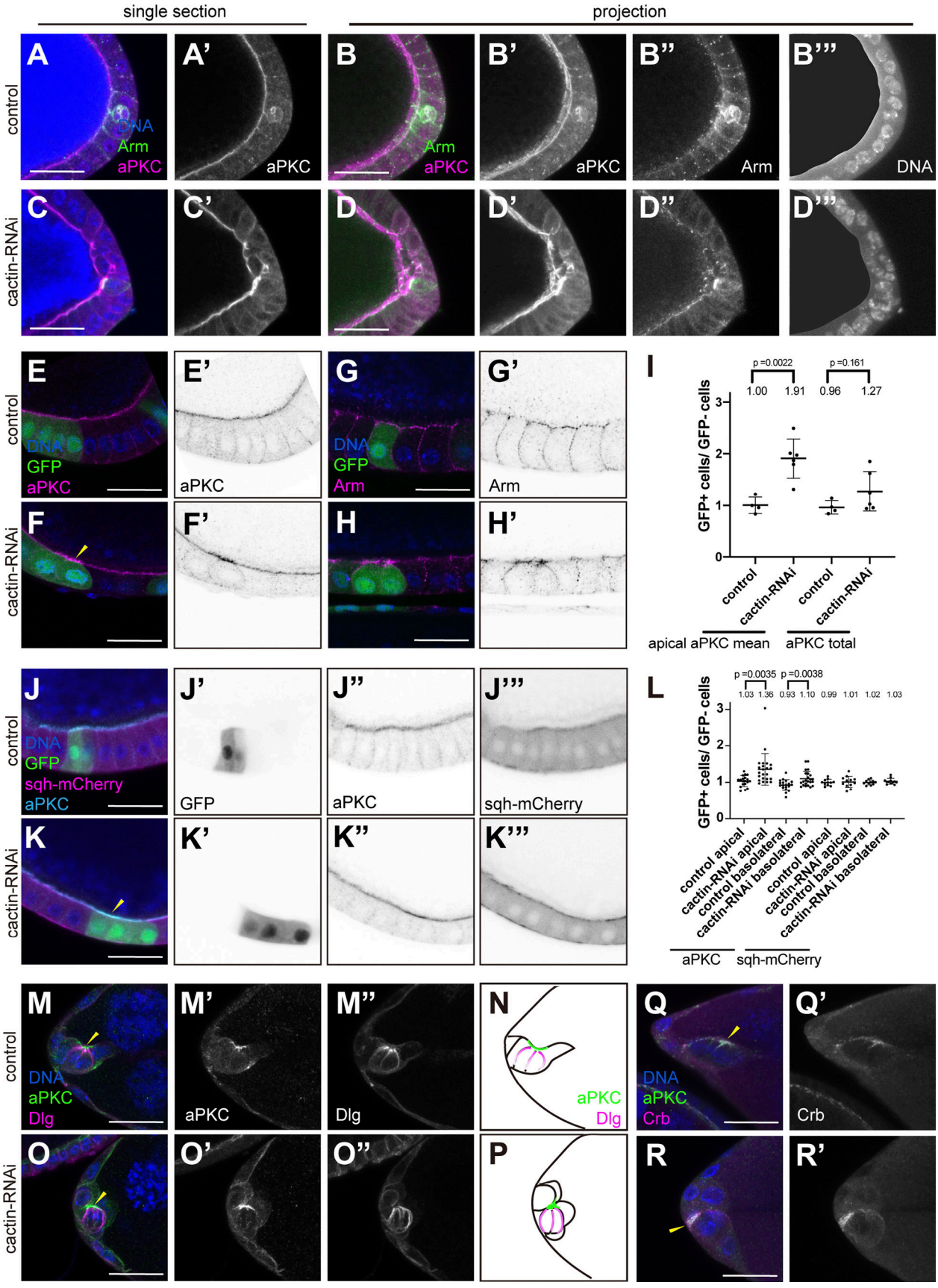

Figure 3. **Excess apical aPKC and apical constriction in Cactin knockdown cells. (A–D‴)** Images of anti-Arm and anti-aPKC co-staining of posterior follicle cells with c306-Gal4 driving UAS-LifeAct-GFP together with (A–B‴) control (crossed to *w1118*) or (C–D‴) UAS-*cactin*-RNAi. **(A, A′, C, and C′)** Single section

view. **(B–B‴ and D–D‴)** Projection view. Note that in B‴ and D‴, to show the DNA signal in follicle cells more clearly, the autofluorescence from the yolk was masked in black. **(E–F′ and G–H′) (E–F′)** Anti-aPKC staining and (G–H′) anti-Arm of HS-flp-out clones showing the apical constriction phenotypes in Cactin knockdown follicle cells. **(E, E′, G, and G′)** Control (UAS-*w*-RNAi). **(F, F′, H, and H′)** UAS-*cactin*-RNAi. Arrowhead indicates the apical domain in a *cactin*-RNAi clone. **(E′ and F′)** Images show the aPKC channel in E and F. **(G′ and H′)** Images show the Arm channel in G and H. **(I)** Quantification of aPKC staining intensity in HS-flp-out clones showing the apical constriction phenotypes. The ratio of aPKC staining intensity in RNAi clones (GFP+ cells)/non-RNAi clones (GFP− cells) is shown. Ratio = 1 suggests that there is no difference between the RNAi clones and the non-RNAi clones. Ratio > 1 suggests RNAi clones have higher levels of aPKC than non-RNAi clones. **(J–K‴)** HS-flp-out clones showing anti-aPKC and anti-mCherry co-staining in follicle cells. GFP (green) labels Gal4-expressing clones. **(J–J‴)** Control (UAS-*w*-RNAi). **(K–K‴)** UAS-*cactin*-RNAi. Arrowhead indicates the aPKC is concentrated in Cactin knockdown cells. **(J′–J‴ and K′–K‴)** Images show the single channels in J and K. **(L)** Quantification of aPKC staining intensity in HS-flp-out clones. The ratio of aPKC staining intensity in RNAi clones (GFP+ cells)/non-RNAi clones (GFP− cells) is shown. **(M–P)** Images of anti-aPKC and anti-Dlg co-staining border cell clusters with c306-Gal4 together with (M) control (cross to *w1118*) or (O) UAS-*cactin*-RNAi. **(M′, M″, O′, and O″)** Images show the single channels in M and O. **(N–P)** Schematic of polarity of the border cell cluster in M–O. **(Q–R′)** Images of anti-aPKC and anti-Crb co-staining border cell clusters with c306-Gal4 together with (Q) control (cross to *w1118*) or (R) UAS-*cactin*-RNAi. **(Q′ and R′)** Images show the anti-Crb single channels in Q and R. Yellow arrowheads indicate the apical junctions in border cell clusters. Scale bars, 20 µm.

delamination and migration with aPKC concentrated on one side of the cluster, especially in polar cells, which have small apical surfaces (arrowhead in Fig. 3, M and M′). The lateral marker Dlg localizes in a distinct domain from aPKC (Fig. 3, M″ and N). In contrast, border cell clusters with Cactin knockdown showed excess aPKC compared to controls (Fig. 3, O and O′), while Cactin knockdown did not significantly alter Dlg (Fig. 3, O″ and P). A second apical marker, Crb, accumulated apically, similar to aPKC (Fig. 3, Q and R′), and showed a 12% increase in apical junctions of Cactin knockdown clusters compared to control (Fig. S3 C). One interpretation of the border cell phenotype is that individual border cells may be apically constricting similar to the most extreme follicle cell clones (Fig. 3, E–H′ and M–R′; and Fig. S3, D–E″). A previous study showed that there are normally two pools of aPKC in border cell clusters: one at apical junctions keeping the cluster collectively polarized and a second in protrusions, especially the lead cell protrusion (Wang et al., 2018). Our results suggest that *cactin*-RNAi disrupts this balance, leading to excess apical aPKC.

Nonmuscle Myosin-II binds actin microfilaments, which drive cell motility, and Myosin-II is required for communication between border cells and coordination of their collective direction sensing (Aranjuez et al., 2016; Mishra et al., 2019; Combedazou et al., 2017). In control border cells, the Myosin-II light chain tagged with mCherry (Sqh::mCherry) accumulates strongly in puncta at the apical polar cell surfaces and transiently at the base of the main border cell protrusion (Mishra et al., 2019) as well as in dynamic cortical flashes around the outside of the cluster (Aranjuez et al., 2016; Fig. S3 F and Video 2). In *cactin*-RNAi–expressing border cells, Sqh::mCherry was distributed in random and dynamic cortical flashes at the periphery of each individual border cell (Fig. S3, G–I and Video 2), suggesting the coordination of individual border cell polarity was disrupted. Thus, fixed and live imaging confirmed a defect in coordination of individual border cell polarities and overall cluster polarization. Border cells may be more sensitive than epithelial follicle cells to loss of polarity because they have fewer neighbors from which to receive polarity cues.

Reducing apical aPKC rescued delamination defects in *cactin*-RNAi

The endocytic recycling machinery is required to regulate the balance between the two pools of Crb and aPKC (Wang et al., 2018). Rab proteins are essential for intracellular trafficking and Rab5 and Rab11 in particular are known to function during border cell migration (Ramel et al., 2013). So, we expressed UAS-YFP-tagged Rab5, Rab7, and Rab11 with c306-Gal4 and UAS-*cactin*-RNAi. Strikingly, overexpression of YFP-Rab5 and YFP-Rab11 but not YFP-Rab7 partially rescued aPKC localization in *cactin*-RNAi egg chambers (Fig. 4, A–D′) and delamination defects (Fig. 4 N). We predicted that overexpression of Rab5 or Rab11 might enhance recycling of aPKC, thus partially reducing the excess apical accumulation of aPKC. Consistent with this idea, when we expressed *cactin*-RNAi in flies heterozygous for an aPKC null mutation, which reduced the aPKC level in border cells, including the apical junctions (Fig. 4, E–F′), the delamination defects were also similarly rescued (Fig. 4 N).

Consistent with the interpretation that Rab5 and Rab11 affect apicobasal polarity and aPKC localization, the expression of a dominant-negative form of Rab5 (Fig. S4, A–B′) or Rab11 (Fig. S4, C–D′) caused aPKC mislocalization and border cell delamination defects resembling those caused by *cactin*-RNAi. Combining Rab5-DN and *cactin*-RNAi caused significant egg chamber lethality and enhanced the follicle cell multilayering defect in those egg chambers that survived (Fig. S5, E–H′). One possibility is that Rab5 and Cactin affect polarity by independent mechanisms and thus produce additive effects. However, since the Cactin RNAi is not a null allele, the interpretation of this genetic interaction is not unambiguous. There is a clear correlation though between excess apical aPKC and border cell delamination defects.

We hypothesized that the excess accumulation of apical aPKC observed in *cactin*-RNAi–expressing cells might also reduce the available basolateral aPKC necessary for protrusions. This pool is difficult to detect by staining, so we asked whether forcing aPKC to basolateral membranes in *cactin*-RNAi–expressing clusters would rescue migration. To relocalize aPKC, we took the advantage of a nanobody-based Grab-FP system (Harmansa et al., 2017; and Fig. 4 G). Briefly, we combined endogenous EGFP-tagged aPKC with a basolateral anti-GFP nanobody (Grab-FP-basal), to relocalize EGFP-aPKC to basolateral membranes (Fig. 4, G–I′). Indeed, in *cactin*-RNAi–expressing clusters (Fig. 4, J and J′), relocalizing aPKC to basolateral membranes (Fig. 4, K and K′) partially rescued migration (Fig. 4 N). Conversely, combining GrabFP-Apical with EGFP-aPKC caused a high level of aPKC to accumulate apically and was sufficient to impair

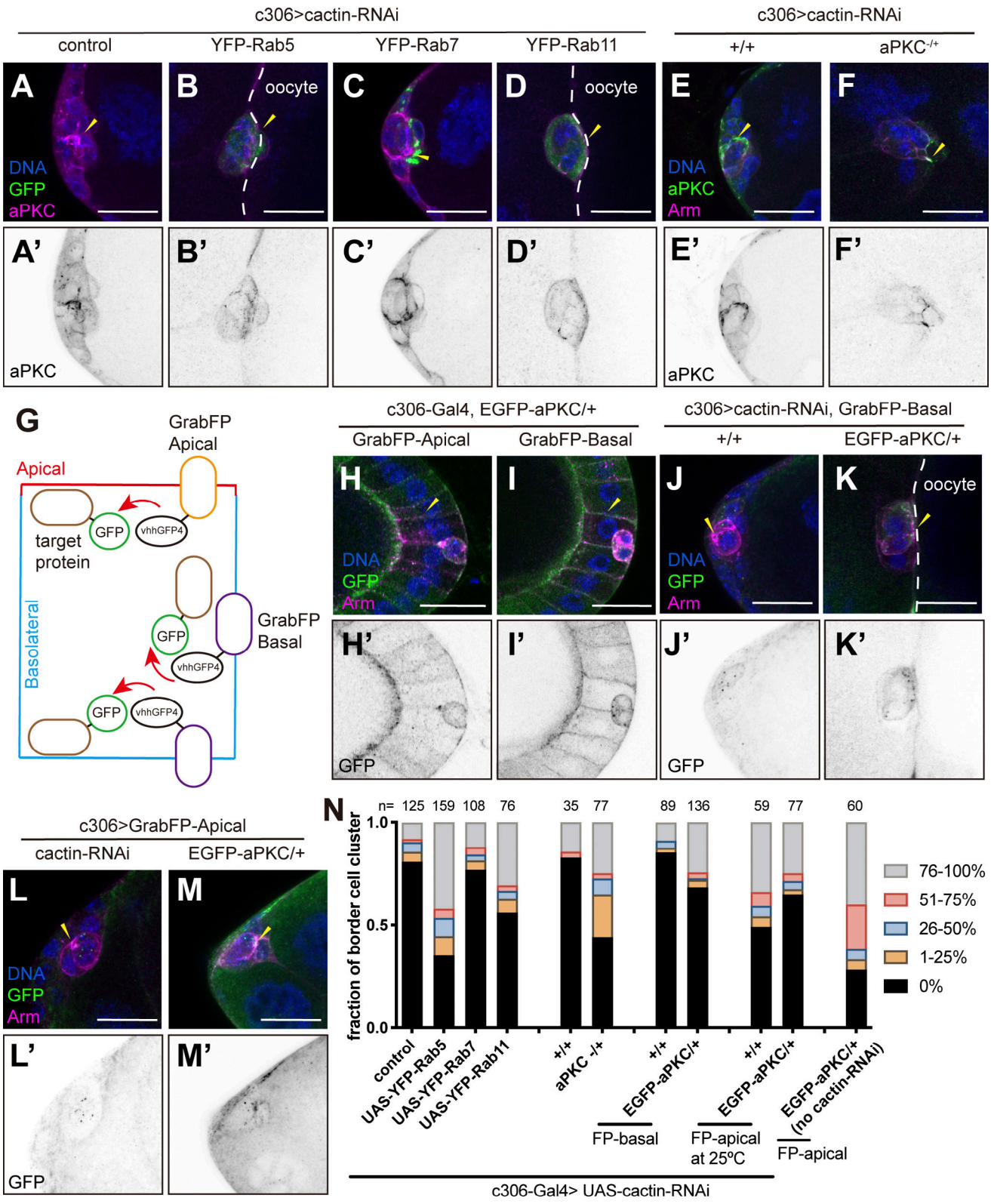

Figure 4. **Delamination is partially rescued by reducing apical aPKC in cactin-RNAi–expressing cells. (A–D)** Images of anti-aPKC staining border cell clusters with c306-Gal4 driven UAS-*cactin*-RNAi with (A) control (crossed to *w1118*), (B) UAS-YFP-Rab5, (C) UAS-YFP-Rab7, or (D) UAS-YFP-Rab11. Yellow arrowheads indicate the apical junctions in the border cell cluster. **(A′–D′)** Images show the single channel of aPKC in A–D. **(E and F)** Images of anti-aPKC and Arm co-staining border cell clusters of c306-Gal4 driven UAS-*cactin*-RNAi together with (E) control (cross to *w1118*) or (F) aPKC null mutant heterozygote. Yellow arrowheads indicate the apical junctions in the border cell cluster. **(E′ and F′)** Images show the single channel of aPKC in E and F. **(G)** Schematic of GrabFP system in which an anti-GFP nanobody is tethered either apically or basolaterally and thereby relocalizes GFP-tagged target proteins to those domains. **(H and I)** Images of posterior follicle cells in egg chambers of c306-Gal4 combined with EGFP-aPKC together with (H) UAS-GrabFP-Apical or (I) UAS-GrabFP-Basal.

Yellow arrowheads indicate the basolateral junctions in the follicle cells. **(H′ and I′)** Images show the single channel of EGFP-aPKC in H and I. **(J and K)** Images of anti-GFP and Arm co-staining border cell clusters of c306-Gal4 driven UAS-*cactin*-RNAi, UAS-GrabFP-Basal together with (J) control (cross to *w1118*) or (K) EGFP-aPKC heterozygote. **(L and M)** Images of anti-GFP and Arm co-staining border cell clusters of c306-Gal4 driven UAS-GrabFP-Apical together with (L) UAS-*cactin*-RNAi or (M) EGFP-aPKC heterozygote. Yellow arrowheads indicate the apical junctions in the border cell cluster. **(J′–M′)** Images show the single channel of anti-GFP in J–M. **(N)** Quantification of delamination defects in stage 10 egg chambers.

delamination (Fig. 4, L–N). These results suggest that the proper level and distribution of aPKC are required for border cell cluster polarization, organization, and delamination.

cactin-RNAi effects on border cell Rac activity

Cactin is conserved from yeast to humans and has been analyzed in multiple organisms. *C. elegans* Cactin was first identified in a genome-wide screen where it was shown to genetically interact with the Rac GTPase MIG-2 and to regulate distal tip cell migration (Cram et al., 2006). Since border cells also require spatiotemporally regulated Rac activity to migrate (Murphy and Montell, 1996; Geisbrecht and Montell, 2004; Wang et al., 2010), we investigated whether Rac activity is affected by *cactin*-RNAi. We combined an established Rac activity sensor (Wang et al., 2010; Cai et al., 2014) with *cactin*-RNAi and used live imaging to monitor Rac activity during delamination. In control border cell clusters, Rac activity is typically elevated in the leading cell as it extends a main protrusion (Mishra et al., 2019; and Fig. S4 I). In contrast, in *cactin*-RNAi, no leading cell protrusion was observed (Fig. S4 J) and the front/back bias of Rac Förster resonance energy transfer (FRET) was correspondingly absent (Fig. S4 K). Interestingly, the total FRET index in *cactin*-RNAi increased by 25% compared to control (Fig. S4 L), suggesting Rac activity is higher in Cactin-depleted border cells, consistent with the study in *C. elegans* (Tannoury et al., 2010). To test whether excess Rac activity contributes to the Cactin knockdown phenotypes, we assessed whether decreasing Rac activity might rescue delamination defects. There are three genes encoding Rac GTPases in *Drosophila,* which are largely functionally redundant in border cells (Geisbrecht and Montell, 2002). When we expressed *cactin*-RNAi in border cells heterozygous for Rac1, Rac2, and Mtl null mutations, no rescue was observed (Fig. S4 M). We also found that homozygous Rac2 and Mtl double mutants, though normally viable, died when combined with *cactin*-RNAi (Fig. S4 M), again showing that reduction in Rac does not ameliorate *cactin*-RNAi. These results suggest that although Cactin knockdown causes a small increase in Rac activity, this effect does not seem to account for the delamination defect. In further support of this interpretation, Rac overexpression causes defects that are distinct from *cactin*-RNAi in that cluster organization is normal.

Cactin regulates aPKC and Crb localizations via its spliceosome function

Although diverse functions have been ascribed to Cactin, its most conserved role appears to be as a component of the eukaryotic spliceosome (Baldwin et al., 2013; Zanini et al., 2017; Thakran et al., 2018; Fica et al., 2019; Cecchetelli et al., 2016; Doherty et al., 2014). However, its role in splicing has not yet been demonstrated in *Drosophila* or associated with cell migration. Specifically, Cactin is a component of the C complex, which carries out the second catalytic step of intron removal, after the B* complex (Matera and Wang, 2014). To test whether Cactin's spliceosome function is required for border cell delamination, we performed an RNAi screen of other spliceosome complex C components in *Drosophila* (http://flybase.org/reports/FBgg0000536.html). We tested 103 lines corresponding to 70 genes. Of the 71 lines (targeting 56 genes) that were viable when expressed with c306-Gal4, so border cell migration could be evaluated, 18 (17 genes) caused >10% incomplete migration (Fig. 5, A–G). Importantly, these RNAi lines caused delamination and cluster morphology defects similar to the *cactin*-RNAi, with aPKC abnormally concentrated in apical junctions (Fig. 5, A–G). This phenotype has not been reported for other border cell mutants or knockdowns. Multiple layers of follicle cells were also observed (Fig. S5, A–B″). These results suggest that Cactin most likely regulates aPKC and Crb localization via its spliceosome function.

We then asked whether Cactin knockdown alters aPKC and Crb alternative splicing directly, as both aPKC and Crb are alternatively spliced (Kumichel et al., 2015; Xu et al., 2014; and Fig. S5 C). We performed quantitative RT-PCR (qRT-PCR) and compared both the overall levels of aPKC and Crb mRNA between control and *cactin*-RNAi (Fig. S5, C and D) as well as the proportions of different isoforms (Fig. 5, H–K). To our surprise, the isoform proportions were not significantly altered; rather the overall mRNA levels were increased. Rab5 and Rab11 mRNA levels were unchanged in *cactin*-RNAi, consistent with the idea that Cactin and the Rab GTPases regulate aPKC localization independently of one another (Fig. 5 L).

The Cactin knockdown phenotype was surprisingly specific considering that most genes are spliced and reduction of a core splicing factor is likely to impact many cellular functions. To assess whether Cactin regulates the splicing of a few relevant target mRNAs or is required more globally, we performed RNA sequencing (RNA-seq) on ovaries from control (UAS-GFP-RNAi) and UAS-*cactin*-RNAi and compared the mRNA levels and isoform profiles using CY2-Gal4 (Miao et al., 2020) to drive the RNAi lines in all follicle cells. We found 289 genes, which represent <10% of the roughly 8,000 expressed genes, whose isoform proportions changed significantly in *cactin*-RNAi (Table S1). This result shows that although Cactin functions as a general splicing factor, the knockdown does not affect all spliced mRNAs equally.

Gene ontology and pathway analyses did not reveal specificity in the set of affected genes (Table S2). However, among the 289 genes, we found four that are known to regulate aPKC and/or Crb apical localization in *Drosophila*: Glaikit (*gkt*), a member of the phospholipase D superfamily, localizes Crb to the apical membrane during *Drosophila* embryogenesis (Dunlop et al.,

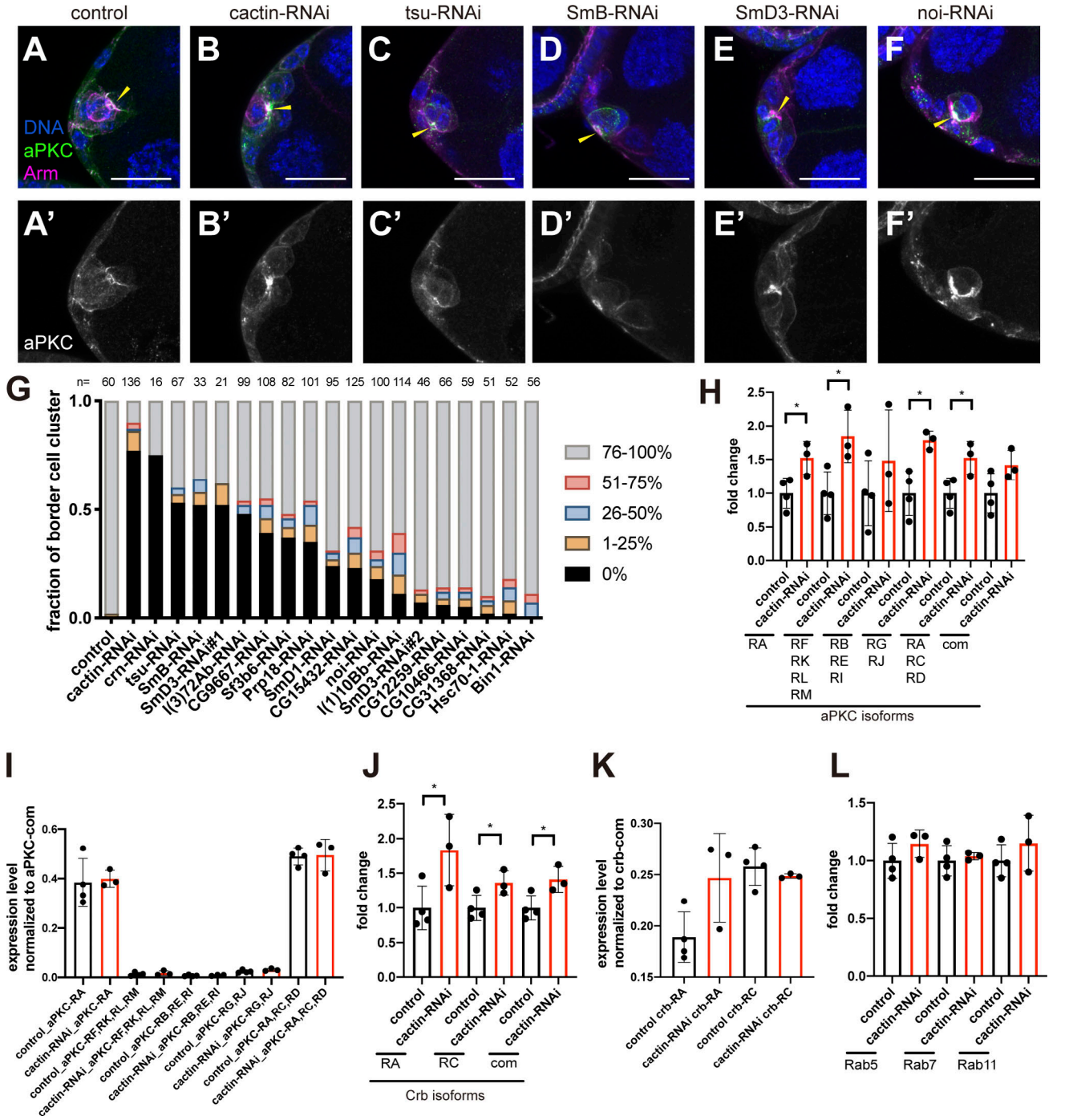

Figure 5. **Cactin regulates aPKC and Crb localizations via its spliceosome function. (A–F)** Representative images of egg chambers expressing RNAi against the indicated spliceosome complex components. Anti-aPKC and anti-Arm co-staining c306-Gal4 border cell clusters together with (A) control (crossed to *w1118*), (B) UAS-*cactin*-RNAi (as a positive control), (C) UAS-*tsu*-RNAi, (D) UAS-*SmB*-RNAi, (E) UAS-*SmD3*-RNAi, or (F) UAS-*noi*-RNAi. Yellow arrowheads indicate the aPKC accumulation in the apical junctions. **(A′–F′)** Images show the single channel of anti-aPKC in A–F. Scale bars, 20 µm. **(G)** Quantification of delamination defects in stage 10 egg chambers. c306-Gal4 crosses to w1118 used as the negative control and c306-Gal4 driven UAS-*cactin*-RNAi used as the positive control. **(H)** mRNA fold change of aPKC isoforms assessed by qPCR. Each dot represents an independent biological replicate. **(I)** Proportion of mRNA levels of different aPKC isoforms. mRNA levels of aPKC isoforms were normalized to aPKC_com, which detected all aPKC isoforms. Each dot indicates an independent biological replicate in the qRT-PCR. **(J)** mRNA fold change of Crb isoforms. **(K)** Proportion of mRNA levels of different Crb isoforms. **(L)** mRNA fold change of Rab5/7/11. Controls are shown in black bars; cactin-RNAis are shown in red bars. Asterisks indicate $P < 0.05$.

2004); Twins (*tws*), a *Drosophila* B-type protein phosphatase 2A subunit, forms a complex with aPKC and is required to maintain aPKC in apical junctions in larval neuroblasts (Chabu and Doe, 2009); Sec23 (also known as *haunted*) and Sec24CD (also known as *ghost*) promote transit of Crb from the ER to the Golgi and thus regulate the amount of Crb that reaches the apical plasma membrane (Kumichel et al., 2015). The overall mRNA levels of these genes did not show significant differences between control and *cactin*-RNAi (Fig. 6 A). However, specific isoforms of Sec23 and Sec24CD, Sec23-RD and Sec24CD-RA, showed higher expression in *cactin*-RNAi (Fig. 6 B; and Fig. S5, E and F). *Cactin*-RNAi cells also contained a higher proportion of these isoforms relative to all isoforms when compared to control cells (Fig. 6 C; and Fig. S5, E and F). Therefore, the overexpression of specific Sec23 and Sec24CD isoforms may cause excess apical Crb in *cactin*-RNAi–expressing cells, which would in turn lead to excess aPKC. This model predicts that reducing the expression of Sec 23 or Sec24CD might ameliorate the *cactin*-RNAi phenotypes. To test this possibility, we combined *cactin*-RNAi with heterozygotes containing one copy of a Sec23 or Sec24CD null mutant. Remarkably, Sec23 or Sec24CD null mutant heterozygotes partially rescued delamination defects in *cactin*-RNAi (Fig. 6, D and E) whereas neither *gkt*-RNAi nor tws null mutant heterozygotes had a significant effect. Thus, multiple independent genetic manipulations that reduce apical aPKC and/or Crb provided partial rescue of the *cactin*-RNAi cluster polarization and delamination defect (Fig. 6, F–I).

Discussion

Collective polarization of border cells requires Cactin

Collective cell migration is a fundamental cell behavior in normal development and cancer metastasis. While many studies have focused on motility and chemotaxis mechanisms, less is known about how cells detach collectively from an epithelium to initiate migration—the process of delamination. In this work, we used the *Drosophila* border cell system to study the regulation of delamination.

During development, epithelial cells like neural crest precursors undergo an EMT and individualize to become migratory (Piacentino et al., 2020). These cells downregulate E-cadherin and dismantle apical–basal polarity (Sauka-Spengler and Bronner-Fraser, 2008). However, some collectively migrating cells, including border cells, retain coordinated apicobasal polarity, even as they delaminate (Niewiadomska et al., 1999). Border cell cluster apicobasal polarity is required to maintain cluster cohesion during migration, and knockdown of the apical PAR3 or PAR6 proteins causes the cluster to split apart (Pinheiro and Montell, 2004). Border cell delamination is initiated when the outer, migratory cells begin to round up and one or two cells extend large protrusions between the anterior nurse cells. As one cell takes the lead, and the cluster moves out of the epithelium, the cells detach from the basement membrane that surrounds the egg chamber and from the anterior follicle cells that stay behind. Prior to delamination, all apical follicle cell surfaces contact the nurse cells, lateral surfaces contact neighboring follicle cells, and basal surfaces contact the basement membrane. As the border cell cluster delaminates, the cluster turns such that the shared apical surface becomes oriented approximately orthogonal to the direction of migration. In contrast, Cactin knockdown clusters did not carry out this coordinated, collective delamination. In *cactin*-RNAi-expressing clusters, individual border cells still rounded up and surrounded the polar cells, and individual cells moved rapidly within the cluster. However, the cells no longer moved cooperatively as a cluster and no cell extended a large, forward-directed protrusion or took the leading position. Instead, Crb and aPKC appeared overly concentrated at the border cell/polar cell interface and lacking from border cell/border cell junctions.

Prior work has shown that the lead cell usually communicates overall cluster polarization to the following cells (Montell et al., 2012). In the absence of shared apicobasal polarity, Cactin knockdown cells do not appear to be able to produce a lead cell protrusion or coordinate the directional motility of individual cells. The observation that restoring shared apicobasal polarity at least partially rescues delamination and migration suggests that this lack of coordinated polarity contributes significantly to the Cactin knockdown phenotype.

Within the follicular epithelium, clones of *cactin*-RNAi–expressing follicle cells exhibited excess Crb and aPKC and in extreme cases apical constriction. Crb is known to promote tracheal cell apical constriction during tracheal placode invagination, and overexpression of Crb leads to enlarged tracheal pits, where more cells initiate internalization, and to precocious and ectopic epidermal depressions (Letizia et al., 2011). A role for Crb and aPKC in apical constriction has also been observed during morphogenesis of the amnioserosa in the fly embryo (David et al., 2010). In contrast, border cell delamination is distinct from invagination and is inhibited by excess apical Crb and aPKC.

Consistent with the idea that excess apical border cell aPKC impairs border cell delamination, apical targeting of extra aPKC in border cells using the Grab-FP system was sufficient to impair delamination and migration. Moreover, multiple genetic manipulations that reduced apical aPKC and/or Crb in *cactin*-RNAi–expressing border cells rescued delamination and migration. For example, relocalizing aPKC to basolateral surfaces partially rescued the phenotype, as did expressing *cactin*-RNAi in flies heterozygous for mutations in aPKC or Sec23 or Sec24CD or overexpressing Rab5 or Rab11 (Fig. 6, F–I). Our work thus suggests that achieving the proper level and localization of aPKC is required to maintain coordinated cluster polarity, which is required for the delamination process.

Although Cactin-knockdown epithelial follicle cells show an increase in apical aPKC and Crb, the epithelium appears relatively normal and functions, whereas border cell delamination and migration are severely impaired. Border cells may be more sensitive to perturbations of apicobasal polarity because they have fewer polarity cues than cells within the epithelium. For example, border cells lack the basal cue from attachment to the basement membrane and lateral cues from connections to follicle cell neighbors.

Drosophila Cactin functions as a spliceosome C component

Cactin is conserved in organisms as diverse as fungi, plants, and animals, suggesting it serves a fundamental cell biological

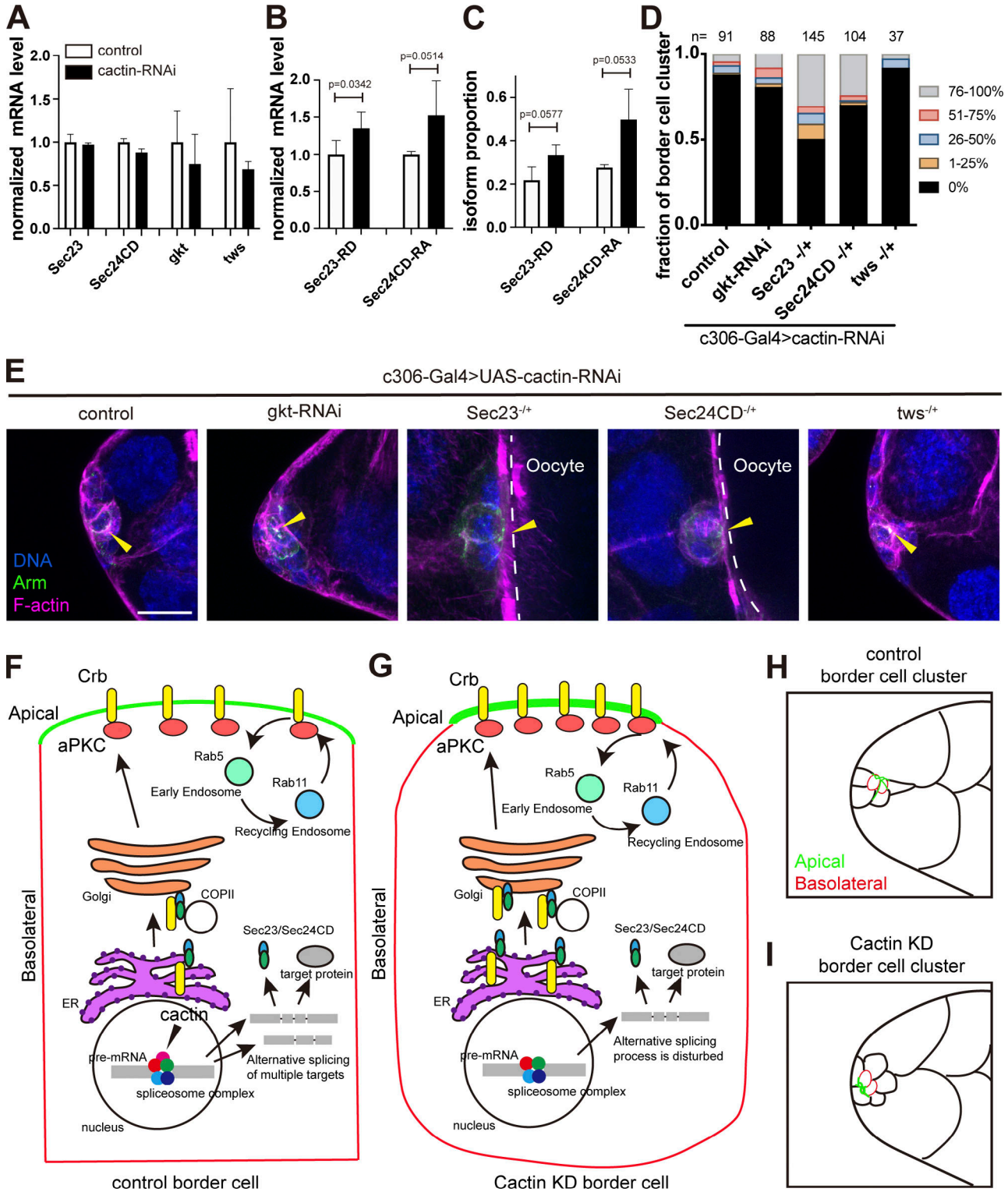

Figure 6. **Sec23 or Sec24CD null heterozygotes partially rescue cactin-RNAi delamination defects. (A)** Normalized expression of Sec23, Sec24CD, gkt, and tws (for all isoforms). **(B)** Normalized expression of Sec23-RD and Sec24CD-RA (isoforms highly expressed in *cactin*-RNAi compared to control). In each case, the mean expression level in the control is set to one and the expression level in *cactin*-RNAi is normalized to the mean of the control. **(C)** Proportion of mRNA levels of Sec23-RD and Sec24CD-RA isoforms in all isoforms. **(D)** Quantification of delamination defects in stage 10 egg chambers. **(E)** Images of border cell clusters of c306-Gal4 driven UAS-*cactin*-RNAi together with control (cross to *w1118*), *gkt*-RNAi, Sec23 null mutant heterozygote, Sec24CD null mutant heterozygote, and tws null mutant heterozygote. Yellow arrowheads indicate the apical junctions in the border cell clusters. Scale bars, 20 µm. **(F and G)** Schematic of working models showing how Cactin regulates aPKC and Crb apical localizations. **(F)** Model showing expression and trafficking of Crb and aPKC in control cells. **(G)** Model showing accumulation of excess apical Crb and aPKC in a Cactin knockdown border cell. **(H and I)** Schematic drawing showing how Cactin knockdown disturbs border cell organization and delamination. **(H)** Control border cell cluster. **(I)** Cactin knockdown border cell cluster.

function. Consistent with that idea, in numerous organisms, Cactin has been found to physically associate with the spliceosome C complex, which catalyzes the second step of intron removal (Matera and Wang, 2014). Even though the fly studies described to date had not yet connected Cactin to the spliceosome, our data suggest that in flies too, Cactin serves as a spliceosome C component because knockdowns of multiple spliceosome C component proteins cause similar border cell delamination defects.

It is striking that knockdown of general splicing factors like Cactin causes a relatively specific defect in collective border cell polarization and migration. The RNA-seq analysis demonstrates widespread changes in abundance of numerous mRNA isoforms. These changes are likely due to a combination of direct effects on splicing and indirect effects. For example, the splicing of multiple transcription factors is dysregulated, which could lead to observed changes in mRNA abundances, including the observed increases in Sec23 and Sec24CD isoforms. Although many genes are affected upon Cactin knockdown, we were nevertheless able to show functional significance of those that regulate aPKC and/or Crumbs apical accumulation.

Mutations in general splicing factors also cause specific defects in humans and can lead to cell-type–specific diseases. For example, mutations in several genes encoding spliceosomal proteins cause autosomal dominant retinitis pigmentosa, indicating that human retinal cells are especially sensitive to splicing defects although the mechanistic basis for the sensitivity is not known (Matera and Wang, 2014). Photoreceptor cells have enormous apical domains with extensive invaginations—the rod and cone outer segments. The work described here shows that disrupted apicobasal polarization is one mechanism by which mutation of a general splicing factor can lead to a cell-type–specific defect in cells with specialized polarity requirements.

Materials and methods

Key resources

Key resources are listed in Table 1.

Fly husbandry

Files were kept at 25°C, 80% humidity on a 12-h light/dark cycle unless otherwise noted. For RNAi knockdown experiments, 2–4-d-old females were kept in 29°C for 2 d, then transferred to a vial with dry yeast and further kept in 29°C overnight before dissection. For clonal analyses (heat shock flpout clones), 2–4-d-old females were heat-shocked for 1 h at 37°C to induce clones, then transferred to a vial with dry yeast at 25°C for 3 d before dissection.

Detailed fly genotypes in each figure are listed in Table 2.

Generation of UAS-*cactin* and UAS-*cactin*-RFP transgenic lines

To generate UAS-*cactin* clones, the *cactin*-cDNA fragment was amplified from a DGRC cDNA (LP09118) and subcloned into a pUAST-attB vector using EcoRI and XbaI sites. To generate the UAS-*cactin*-RFP clone, the UAS-R-*Inx2*-RFP vector (Miao et al., 2020) was digested with EcoRI and BsrGI to remove the Inx2 cDNA fragment. The same *cactin*-cDNA fragment described above was subcloned to the vector with EcoRI and BsrgI sites. The clones were sequence-verified, and transgenic lines were established through ΦC-31 integrase mediated transformation (Bestgene). The attP2 site was used (Bloomington *Drosophila* Stock Center [BDSC]: 8622).

Immunostaining and imaging

Adult female ovaries were dissected in Schneider's medium (Thermo Fisher Scientific) with 20% fetal bovine serum. Ovarioles were immediately fixed for 20 min in 4% paraformaldehyde at room temperature. After fixation, ovarioles were washed with PBS/0.1% Triton X-100 (PBST) four times (15 min each), and then incubated with primary antibodies overnight at 4°C. The following day, ovarioles were washed with PBST four times (10 min each) before incubation in the secondary antibody for 2 h at room temperature. After removal of secondary antibodies, samples were washed with PBST four times (10 min each) and then stored in Vectashield (Vector Laboratories) at 4°C before mounting. The following antibodies were used in this study: rat anti-E-cadherin (1:50, DCAD2; Developmental Studies Hybridoma Bank [DSHB]), mouse anti-Armadillo (1:75, N2.7A1; DSHB), mouse anti-Cactus (1:100; DSHB), mouse anti-Dorsal (1:100; DSHB), mouse anti-Crumbs (1:10, cq4; DSHB), mouse anti-Dlg (1:20; DSHB), rabbit anti-mCherry (1:500; Novus) rabbit anti-aPKC (1:200; Santa Cruz), rabbit anti-GFP (1:300; Lifetech), Hoechst (1:1,000), Alexa 488, 568, 633 (1:300; Lifetech), phalloidin 488, 568 (1:300; Lifetech). Images were taken on a Zeiss LSM 780 or 800 confocal microscope, using a 20 × 1.2 NA objective or 40 × 1.4 NA water objective. Z-stacks covering the egg chambers were taken with a 1-µm step size for border cell clusters.

Live imaging

For live imaging, ovaries were dissected in Schneider's medium (Thermo Fisher Scientific) with 20% fetal bovine serum. Individual ovarioles were carefully pulled out and stage 10 or older egg chambers were removed. The egg chambers were collected in a 1.7-ml tube and washed with dissecting medium twice, then added 200 µl dissecting medium with insulin (200 µg/ml) and 1% low melt agarose. 90 µl medium with the egg chambers then was mounted on a 50-mm Lumox dish. Time-lapse imaging was performed using a 40 × 1.4 NA water immersion objective. The 1-µm-thick z-sections including the entire border cell cluster were collected at 1-min or 2-min intervals.

Quantification of border cell migration index

For quantification of border cell migration, stage 10B egg chambers were imaged at 20× magnification. Z-stacks projection images of LifeAct-GFP or anti-Arm were used to analyze the position of the border cell cluster.

Quantification of 10XSTAT-GFP intensity

From the SUM intensity Z-stack images of the anterior end of stage 8 egg chambers, the threshold was adjusted in the GFP channel (ImageJ function: Image > Adjust > Threshold) and background subtracted in FIJI. Then the three cells adjacent to the polar cells (based on the Arm channel) were selected and the GFP intensity was measured.

Table 1. **Key resources**

Reagent or resource	Source	Identifier
Antibodies		
Alexa Fluor 568 phalloidin (1:500 dilution)	Thermo Fisher Scientific	Cat#A12380
Mouse monoclonal anti-Arm (1:75 dilution)	DSHB	DSHB Cat#N2.7A1; RRID: AB_528089
Rat monoclonal anti-Ecad (1:50 dilution)	DSHB	DSHB Cat#DCAD2; RRID: AB_528120
Rabbit polyclonal anti-GFP (1:300 dilution)	Invitrogen	Cat#A10260; RRID: AB_2534022
Rabbit polyclonal anti-mCherry (1:500 dilution)	Novus Bio-logicals	Cat#NBP2-25157
Mouse monoclonal anti-Cactus (1:10 dilution)	DSHB	DSHB Cat#anti-cactus 3H12; RRID: AB_528109
Mouse monoclonal anti-Dorsal (1:10 dilution)	DSHB	DSHB Cat#anti-dorsal 7A4; RRID: AB_528204
Mouse monoclonal anti-FasIII (1:10 dilution)	DSHB	DSHB Cat#7G10 anti-Fasciclin III; RRID: AB_528238
Mouse monoclonal anti-Dlg (1:10 dilution)	DSHB	DSHB Cat#4F3 anti-discs large; RRID: AB_528238
Mouse monoclonal anti-Crb (1:10 dilution)	DSHB	DSHB Cat#cq4; RRID: AB_528181
Rabbit anti-aPKC (1:200 dilution)	Santa Cruz Biotech-nology	Cat#sc-216
Chemicals, peptides, and recombinant proteins		
Hoechst 33342	Sigma-Aldrich	Cat# 14533
Experimental models: organisms/strains		
D. melanogaster: c306-Gal4: P{w[+mW.hs]=GawB}c306, w[1118]	BDSC	FBti0003935 RRID: BDSC_3743
D. melanogaster: y[1] w[*]; P{y[+t*] w[+mC]=UAS-Lifeact-GFP}VIE-260B	Hatan et al. (2011)	FBtp0064437
D. melanogaster: w[1118]	BDSC	FBst0003605 RRID: BDSC_3605
D. melanogaster: RNAi of Cactin: w^{1118}; P{GD9200}v32718	Vienna *Drosophila* Resource Center	FBti0098576 RRID: v32718
D. melanogaster: RNAi of Cactin w^{1118}; P{GD9200}v32719	Vienna *Drosophila* Resource Center	FBti0098576 RRID: v32719
D. melanogaster: RNAi of Cactin P{KK100507}VIE-260B	Vienna *Drosophila* Resource Center	FBti0116514 RRID: v106979
D. melanogaster: P{tubP-GAL80^{ts}}2	BDSC	FBti0027797 RRID: BDSC_7017
D. melanogaster: UAS-Cactin	This work	N/A
D. melanogaster: UAS-Cactin-RFP	This work	N/A
D. melanogaster: P{UAS-mCherry.CAAX.S}2	BDSC	FBti0164914 RRID: BDSC_59021
D. melanogaster: Fruitless-Gal4	Borensztejn et al. (2013)	N/A
D. melanogaster: Upd-Gal4: P{GawB}E132, w*	BDSC	FBti0002638 RRID: BDSC_26796
D. melanogaster: RNAi of white: y[1] v[1]; P{y[+t7.7] v[+t1.8]=TRiP.HMS00017}attP2	BDSC	FBst0033623 RRID: BDSC_33623
D. melanogaster: Hsflp; AY-Gal4, UAS-GFP	D. Montell lab stock	N/A
D. melanogaster: w[1118]; P{10XStat92E-GFP}1	BDSC	FBst0026197 RRID: BDSC_26197
D. melanogaster: UAS-cactus: M{UAS-cact.ORF.3xHA} ZH-86Fb	FlyORF	FBti0153388
D. melanogaster: w[*]; P{w[+mC]=sqh-mCherry.M}3	BDSC	FBst0059024 RRID: BDSC_59024
D. melanogaster: y^1 w*; P{UASp-YFP.Rab5}02	BDSC	FBti0100788 RRID: BDSC_24616

Table 1. **Key resources (*Continued*)**

Reagent or resource	Source	Identifier
D. melanogaster: y^1 w*; P{UASp-YFP.Rab7}$vig2^{18}$	BDSC	FBst0023270 RRID: BDSC_23270
D. melanogaster: y^1 w*; P{UASp-YFP.Rab11}sra^{32}/TM3, Sb^1	BDSC	FBst0009790 RRID: BDSC_9790
D. melanogaster: apkc mutant: $\underline{y}^1$ w^{67c23}; P{lacW}$aPKC^{k06403}$/CyO	BDSC	FBst0010622 RRID: BDSC_10622
D. melanogaster: EGFP-aPKC	Chen et al. (2018)	FBti0211865
D. melanogaster: UAS-GrabFP-Apical: M{lexAop-UAS-GrabFP.A.Int.mCh}ZH-86Fb	BDSC	FBti0187198 RRID: BDSC_68178
D. melanogaster: UAS-GrabFP-Basal: M{lexAop-UAS-GrabFP.B.Int.mCh}ZH-86Fb	BDSC	FBst0068175 RRID: BDSC_68175
D. melanogaster: UAS-Rac-FRET: P{w[+mC]=UAS-YPet-PAK-RAC-CFP.FRET}3	BDSC	FBst0031431 RRID: BDSC_31431
D. melanogaster: Rac2 mutant: Rac2[Delta] ry[506]	BDSC	FBst0006675 RRID: BDSC_6675
D. melanogaster: Mtl mutant: y[1] w[*]; P{ry[+t7.2]=neoFRT}82B Mtl[Delta]/TM3, Sb[1]	BDSC	FBst0006676 RRID: BDSC_6676
D. melanogaster: Rac1 Rac2 Mtl mutant: y[1] w[*]; Rac1[J11] Rac2[Delta] P{w[+mW.hs]=FRT(w[hs])}2A Mtl[Delta]/TM6B, Tb[1]	BDSC	FBst0006678 RRID: BDSC_6678
D. melanogaster: y^1 w*; P{UASp-YFP.Rab5.S43N}$Eip75B^{02}$/TM3, Sb^1	BDSC	FBst0009772 RRID: BDSC_9772
D. melanogaster: y^1 w*; P{UASp-YFP.Rab11.S25N}06	BDSC	FBst0023261 RRID: BDSC_23261
D. melanogaster: RNAi of tsu y1 v1; P{TRiP.HM05166}attP2	BDSC	FBst0028955 RRID: BDSC_28955
D. melanogaster: RNAi of SmB y1 v1; P{TRiP.HM05097}attP2	BDSC	FBst0028887 RRID: BDSC_28887
D. melanogaster: RNAi of SmD3 y1 sc* v1 sev21; P{TRiP.HM05226}attP2	BDSC	FBst0030534 RRID: BDSC_30534
D. melanogaster: RNAi of noi y1 sc* v1 sev21; P{TRiP.HMS00163}attP2	BDSC	FBst0034845 RRID: BDSC_34845
D. melanogaster: RNAi of gkt y[1] v[1]; P{y[+t7.7] v[+t1.8]=TRiP.HMJ24083}attP40	BDSC	FBst0062874 RRID: BDSC_62874
D. melanogaster: Sec23 mutant ru[1] h[1] Diap1[1] st[1] Sec23[9G] cu[1] sr[1] e[s] ca[1]/TM3, Sb[1] Ser[1]	BDSC	FBst0003094 RRID: BDSC_3094
D. melanogaster: Sec24CD mutant cn[1] Sec24CD[1] bw[1] speck[1]/CyO	BDSC	FBst0003264 RRID: BDSC_3264
D. melanogaster: tws mutant P{ry[+t7.2]=PZ}tws[02414] ry[506]/TM3, ry[RK] Sb[1] Ser[1]	BDSC	FBst0011568 RRID: BDSC_11568
Oligonucleotides		
Primers for PCR out *cactin* cDNA: cactin-F: 5′-TTGGGAATTCGAGCTCATG CCCAAGGAGAAATCCAAGC-3′ cactin-R: 5′-ATCCTCTAGAGGATCTACTAGTCTTA TCGATTCACCGCCTGTAGCGATAGCGCTTGAA-3′	This work	N/A
Primers for qRT-PCR RP49 control: rp49_F: GCTAAGCTGTCGCACAAATG rp49_R: GTTCGATCCGTAACCGATGT	This work	N/A

Table 1. **Key resources (*Continued*)**

Reagent or resource	Source	Identifier
Primers for qRT-PCR Crb isoforms: Crb_comF: CGCTGCAGTTCAAGTACGAG Crb_comR: CGTCCTTGTAGCCAATGTCC Crb_RA-F: GGCTCATCGGGTTACAACTG Crb_RA-R: GTTCCGTTCATGGAGCAAGT Crb_RC-F: CCCCAAGAAAACTGCTTGAA Crb_RC-R: ATTGCAGTTGATGGGTGTCA	This work	N/A
Primers for qRT-PCR aPKC isoforms: aPKC_comF: TCCCGATCAGAACACTGAGG aPKC_comR: CGGGATTCTTGTTGAGGAAA aPKC_N2F: CCCAAGAACCGGCTGTACTA aPKC_N1R: ATCATCCGGGGTCAACTGTA aPKC_N4F: CGTCAGCCATCCCTTCTTTA aPKC_N3R: GTACAGCCGGTTCTTGGGTA aPKC_N6F: TTTACCCGATGGGCAAACTA aPKC_N5R: CTGGAAGATGTGTCCGTTGA aPKC_N7F: AAACGGCCACTTTTATGAGC aPKC_N8F: AGGAGATCGAGCCAGCCTAT aPKC_N10F: AACGATCCCTGCACCATATC aPKC_N9R: GCCATCGCAAGACAATCC	This work	N/A
Primers for qRT-PCR Rab5/7/11: rab5F: CGGCCTTTCTGACACAGACT rab5R: CCTGCGCTCCTCGATAATAC rab7F: CACGATCGGAGCTGATTTCT rab7R: TAGACAAGCACGCAGCAGTC rab11F: CCGGTGTTGGCAAAAGTAAT rab11R: TCCCAGATTTGCGCTTTAAT	This work	N/A
Recombinant DNA		
Plasmid: pUAST-attB	https://www.flyc31.org	GenBank EF362409.1
Software and algorithms		
FIJI	PMID: 22743772	https://fiji.sc/
Adobe Illustrator CC	Adobe	N/A
Prism 8 GraphPad	GraphPad Software	https://www.graphpad.com/scientific-software/prism/

Quantification of aPKC, Crb, sqh-mCherry, Arm expression in *cactin*-RNAi clones

For quantification of staining level, 40× magnification SUM intensity projection images of anti-aPKC, Crb, sqh-mCherry and Arm channel were measured in FIJI. Threshold was adjusted for the channels (ImageJ function: Image > Adjust > Threshold) to subtract background. The apical and basal regions were selected manually. The mean intensity was used as the readout of expression. Except in Fig. 3 I, the total aPKC was equal to mean intensity × apical selected region.

qRT-PCR

For each genotype (Control: CY2-Gal4>UAS-GFP-RNAi; *cactin*-RNAi: CY2-Gal4>UAS-*cactin*-RNAi), 15 pairs of ovaries were dissected from 2–4-d-old females. Total RNA was extracted using the RNeasy kit (Qiagen). Turbo DNase (Thermo Fisher Scientific) was used to remove genomic DNA. Reverse transcription was carried out using the SuperScript III First-Strand Synthesis System (Thermo Fisher Scientific). qRT-PCR was carried out using SsoAdvanced Universal SYBR Green Supermix (Bio-Rad) on Bio-Rad CFX96 real-time PCR detection system. The data were collected using Bio-Rad CFX Manager software (Version 3.1, Bio-Rad). The primers used for qRT-PCR were listed in Table 1.

RNA-seq

For each genotype (Control: CY2-Gal4>UAS-GFP-RNAi; *cactin*-RNAi: CY2-Gal4>UAS-*cactin*-RNAi), three biological replicates were prepared. For each replicate, 20 pairs of ovaries were dissected from 2–4-d-old females. Total RNA extraction and sequencing steps were carried out using Genewiz.

Trimmed reads were mapped to the *Drosophila* genome by HISAT2. *Drosophila* reference genome indices were downloaded from http://daehwankimlab.github.io/hisat2/download/#d-melanogaster, and the *genome_tran* was used. Transcript assembly was permitted by stringtie (Drosophila_melanogaster.BDGP6.32.104.gtf). Estimated transcript abundances in this way were used for further differential gene and isoform analysis.

Table 2. **Fly genotypes**

Figure	Genotypes
Fig. 1, A–D′	c306-Gal4, UAS-LifeActGFP/+, Gal80ts
Fig. 1, E–H′	c306-Gal4, UAS-LifeActGFP/UAS-*cactin*-RNAi, Gal80ts
Fig. 1 M	c306-Gal4, UAS-*cactin*-RNAi/UAS-mCherry-CAAX, Gal80ts
Fig. 1 N	c306-Gal4, UAS-*cactin*-RNAi/UAS-*cactin*, Gal80ts
Fig. 1 O	c306-Gal4, UAS-*cactin*-RNAi/UAS-*cactin*-RFP, Gal80ts
Fig. S1 A	c306-Gal4, UAS-LifeActGFP/+, Gal80ts
Fig. S1 B	c306-Gal4, UAS-LifeActGFP/UAS-*cactin*-RNAi (v32718GD), Gal80ts
Fig. S1 C	c306-Gal4, UAS-LifeActGFP/UAS-*cactin*-RNAi (v32719GD), Gal80ts
Fig. S1 D	c306-Gal4, UAS-LifeActGFP/UAS-*cactin*-RNAi (v106976KK), Gal80ts
Fig. S1, E and E′	HSflp; AY-Gal4, UAS-GFP/UAS-*cactin*-RFP, UAS-*w*-RNAi
Fig. S1, F and F′	HSflp; AY-Gal4, UAS-GFP/UAS-*cactin*-RFP, UAS-*cactin*-RNAi
Fig. S2, A and A′	c306-Gal4, 10X STAT-GFP/+, Gal80ts
Fig. S2, B and B′	c306-Gal4, 10X STAT-GFP/UAS-*cactin*-RNAi, Gal80ts
Fig. S2, D and D′	c306-Gal4, UAS-LifeActGFP/+, Gal80ts
Fig. S2, E and E′	c306-Gal4, UAS-LifeActGFP/UAS-*cactus*, Gal80ts
Fig. S2, F and F′	c306-Gal4, UAS-LifeActGFP/UAS-*cactin*-RNAi, Gal80ts
Fig. S2, H–I′	c306-Gal4, UAS-LifeActGFP/+, Gal80ts
Fig. S2, J and J′	c306-Gal4, UAS-LifeActGFP/UAS-*cactin*-RNAi, Gal80ts
Fig. S2, K and K′	c306-Gal4, UAS-LifeActGFP/UAS-*dorsal*-RNAi, Gal80ts
Fig. 2, A–A‴	c306-Gal4, UAS-LifeActGFP/+, Gal80ts
Fig. 2, C–C‴	c306-Gal4, UAS-LifeActGFP/UAS-*cactin*-RNAi, Gal80ts
Fig. 2 E	c306-Gal4, UAS-LifeActGFP/+, Gal80ts
Fig. 2 F	c306-Gal4, UAS-LifeActGFP/UAS-*cactin*-RNAi, Gal80ts
Fig. 3, A–B‴	c306-Gal4, UAS-LifeActGFP/+, Gal80ts
Fig. 3, C–D‴	c306-Gal4, UAS-LifeActGFP/UAS-*cactin*-RNAi, Gal80ts
Fig. 3, E, E′, G, and G′	HSflp; AY-Gal4, UAS-GFP, UAS-*w*-RNAi
Fig. 3, F, F′, H, and H′	HSflp; AY-Gal4, UAS-GFP, UAS-*cactin*-RNAi
Fig. 3, J–J‴	HSflp; AY-Gal4, UAS-GFP, UAS-*w*-RNAi
Fig. 3, K–K‴	HSflp; AY-Gal4, UAS-GFP, UAS-*cactin*-RNAi
Fig. 3, M–M″, Q, and Q′	c306-Gal4, UAS-LifeActGFP/+, Gal80ts
Fig. 3, O–O″, R, and R′	c306-Gal4, UAS-LifeActGFP/UAS-*cactin*-RNAi, Gal80ts
Fig. S3, A–A″	HSflp; AY-Gal4, UAS-GFP, UAS-*w*-RNAi
Fig. S3, B–B″	HSflp; AY-Gal4, UAS-GFP, UAS-*cactin*-RNAi
Fig. S3, D–D″	c306-Gal4, Gal80ts
Fig. S3, E–E″	c306-Gal4, UAS-*cactin*-RNAi, Gal80ts
Fig. S3, F and H–H″	c306-Gal4, sqh-mCherry/+, Gal80ts
Fig. S3, G and I–I″	c306-Gal4, sqh-mCherry/UAS-*cactin*-RNAi, Gal80ts

Table 2. **Fly genotypes (*Continued*)**

Figure	Genotypes
Fig. 4, A and A′	c306-Gal4, UAS-*cactin*-RNAi, Gal80ts
Fig. 4, B and B′	c306-Gal4, UAS-*cactin*-RNAi, UAS-YFP-Rab5/Gal80ts
Fig. 4, C and C′	c306-Gal4, UAS-*cactin*-RNAi, UAS-YFP-Rab7/Gal80ts
Fig. 4, D and D′	c306-Gal4, UAS-*cactin*-RNAi, UAS-YFP-Rab11/Gal80ts
Fig. 4, E and E′	c306-Gal4, UAS-*cactin*-RNAi/+, Gal80ts
Fig. 4, F and F′	c306-Gal4, UAS-*cactin*-RNAi/aPKC^{-}, Gal80ts
Fig. 4, H and H′	c306-Gal4, EYFP-aPKC/+, UAS-GrabFP-Apical
Fig. 4, I and I′	c306-Gal4, EYFP-aPKC/+, UAS-GrabFP-Basal
Fig. 4, J and J′	c306-Gal4, UAS-*cactin*-RNAi/+, UAS-GrabFP-Basal
Fig. 4, K and K′	c306-Gal4, UAS-*cactin*-RNAi/EYFP-aPKC, UAS-GrabFP-Basal
Fig. 4, L and L′	c306-Gal4, UAS-*cactin*-RNAi/+, UAS-GrabFP-Apical
Fig. 4, M and M′	c306-Gal4, EYFP-aPKC/+, UAS-GrabFP-Apical
Fig. S4, A–B′	c306-Gal4, UAS-YFP-Rab5^{S43N}/+, Gal80ts
Fig. S4, C–D′	c306-Gal4, UAS-YFP-Rab11^{S25N}/+, Gal80ts
Fig. S4, E–F′	c306-Gal4, UAS-YFP-Rab5^{S43N}/UAS-*cactin*-RNAi, Gal80ts
Fig. S4, G–H′	c306-Gal4, UAS-YFP-Rab11^{S25N}/UAS-*cactin*-RNAi, Gal80ts
Fig. S4 I	c306-Gal4, UAS-Rac-FRET/+
Fig. S4 J	c306-Gal4, UAS-*cactin*-RNAi/+, UAS-Rac-FRET/+
Fig. 5, A and A′	c306-Gal4, Gal80ts
Fig. 5, B and B′	c306-Gal4, UAS-*cactin*-RNAi/+, Gal80ts
Fig. 5, C and C′	c306-Gal4, UAS-*tsu*-RNAi/+, Gal80ts
Fig. 5, D and D′	c306-Gal4, UAS-*SmB*-RNAi/+, Gal80ts
Fig. 5, E and E′	c306-Gal4, UAS-*SmD3*-RNAi/+, Gal80ts
Fig. 5, F and F′	c306-Gal4, UAS-*noi*-RNAi/+, Gal80ts
Fig. S5, A–A″	c306-Gal4, UAS-*SmD3*-RNAi/+, Gal80ts
Fig. S5, B–B″	c306-Gal4, UAS-*SmB*-RNAi/+, Gal80ts
Fig. 6 E	c306-Gal4, UAS-*cactin*-RNAi/+, Gal80ts
	c306-Gal4, UAS-*cactin*-RNAi/UAS-*gkt*-RNAi, Gal80ts
	c306-Gal4, UAS-*cactin*-RNAi/Sec23^{-}, Gal80ts
	c306-Gal4, UAS-*cactin*-RNAi/Sec24CD^{-}, Gal80ts
	c306-Gal4, UAS-*cactin*-RNAi/tws^{-}, Gal80ts

Differential gene expression analysis was performed with the DEseq2 R package (http://bioconductor.org/packages/devel/bioc/vignettes/DESeq2/inst/doc/DESeq2.html).

Isoform switch analysis was performed with isoformswitchanalysis R package (https://bioconductor.org/packages/devel/bioc/vignettes/IsoformSwitchAnalyzeR/inst/doc/IsoformSwitchAnalyzeR.html).

Gene ontology and pathway analyses were performed with DAVID bioinformatics Resources 6.8 (https://david.ncifcrf.gov/tools.jsp). 286 out of 289 genes were analyzed. Gene ontology of biological pathway, cellular component, and molecular function were analyzed.

Table 3. **Number of samples in figures**

Figure	Numbers of samples (*n*)
Fig. S1 G	Control: 26; *cactin*-RNAi: 30
Fig. S2 C	Control: 31; *cactin*-RNAi: 31
Fig. 3 I	Control: 4; *cactin*-RNAi: 6
Fig. 3 L	For aPKC: Control: 19; *cactin*-RNAi: 23. For sqh-mCherry: Control: 11; *cactin*-RNAi: 12
Fig. S3 C	For Crb: Control: 12; *cactin*-RNAi: 9. For Arm: Control: 12; *cactin*-RNAi: 12
Fig. S4, K and L	Control: 33; *cactin*-RNAi: 30
Fig. 5, H–L	Control:4; *cactin*-RNAi: 3

Statistics and data presentation

Standard statistical tests were performed using Prism 8. Unpaired *t* test (two-tailed) was used for comparing two groups with similar variance as determined by the *F* test. Mann–Whitney nonparametric test (two-tailed) was used for comparing two groups with different variances. Ordinary one-way ANOVA, followed by Tukey's multiple comparisons test, was used for comparing multiple groups with similar variance as determined by Brown–Forsythe test. All graphs were generated using Prism 8. All confocal images belonging to the same experiment were acquired using the exact same settings. For visualization purposes, brightness adjustments were applied using FIJI to the confocal images shown in the figure panels. All quantitative analyses were carried out on unadjusted raw images or sum intensity projections. All fly crosses were repeated at least twice and ovary dissections and staining were repeated at least three times. The exact sample size (*n*) is listed in each figure, representing biological replicates. Sample size was not predetermined by statistical methods, but we used prior knowledge to estimate minimum sample size. The experiments were not randomized. Investigators were not blinded.

Number of samples in each figure are listed in Table 3.

Online supplemental material

Fig. S1 shows multiple *cactin*-RNAi lines cause delamination defects. Fig. S2 shows Cactin functions independently of JAK/STAT or Toll signaling pathways in border cells. Fig. S3 shows excess apical Crb in Cactin knockdown cells. Fig. S4 shows that cactin-RNAi indirectly affects Rac activity in border cells. Fig. S5 shows Cactin regulates aPKC and Crb localizations indirectly via its spliceosome function. Table S1 shows the 289 genes whose isoform proportions changed significantly in *cactin*-RNAi. Table S2 shows the Gene ontology and pathway analyses of the 289 genes. Video 1 shows time-lapse videos of c306-Gal4>UAS-LifeAct-GFP/+ (control, left) and c306-Gal4>UAS-LifeAct-GFP, UAS-*cactin*-RNAi (right). Video 2 shows time-lapse videos of c306-Gal4, sqh-mCherry/+ (control, left) and c306-Gal4>UAS-*cactin*-RNAi/sqh-mCherry (right).

Acknowledgments

We thank D.J. Montell lab members for helpful discussions. We thank Jane Moon for technical support in Fig. S2 G. We thank Yang Hong (University of Pittsburgh, Pittsburgh, PA) for reagents and BDSC and Vienna *Drosophila* Resource Center for fly stocks.

The work was funded by National Institutes of Health grant R01 GM073164 to D.J. Montell.

The authors declare no competing financial interests.

Author contributions: G. Miao and D.J. Montell designed the experiments and coordinated the project. G. Miao performed the experiments, collected, and analyzed the data. L. Guo analyzed the RNA-seq data. G. Miao and D.J. Montell wrote the manuscript.

Submitted: 26 February 2022
Revised: 22 April 2022
Accepted: 9 May 2022

References

Aceto, N., A. Bardia, D.T. Miyamoto, M.C. Donaldson, B.S. Wittner, J.A. Spencer, M. Yu, A. Pely, A. Engstrom, H. Zhu, et al. 2014. Circulating tumor cell clusters are oligoclonal precursors of breast cancer metastasis. *Cell*. 158:1110–1122. https://doi.org/10.1016/j.cell.2014.07.013

Aranjuez, G., A. Burtscher, K. Sawant, P. Majumder, and J.A. McDonald. 2016. Dynamic myosin activation promotes collective morphology and migration by locally balancing oppositional forces from surrounding tissue. *Mol. Biol. Cell*. 27:1898–1910. https://doi.org/10.1091/mbc.E15-10-0744

Au, S.H., B.D. Storey, J.C. Moore, Q. Tang, Y.-L. Chen, S. Javaid, A.F. Sarioglu, R. Sullivan, M.W. Madden, R. O'Keefe, et al. 2016. Clusters of circulating tumor cells traverse capillary-sized vessels. *Proc. Natl. Acad. Sci. USA*. 113:4947–4952. https://doi.org/10.1073/pnas.1524448113

Bach, E.A., L.A. Ekas, A. Ayala-Camargo, M.S. Flaherty, H. Lee, N. Perrimon, and G.-H. Baeg. 2007. GFP reporters detect the activation of the *Drosophila* JAK/STAT pathway in vivo. *Gene Expr. Patterns*. 7:323–331. https://doi.org/10.1016/j.modgep.2006.08.003

Baldwin, K.L., E.M. Dinh, B.M. Hart, and P.H. Masson. 2013. CACTIN is an essential nuclear protein in Arabidopsis and may be associated with the eukaryotic spliceosome. *FEBS Lett.* 587:873–879. https://doi.org/10.1016/j.febslet.2013.02.041

Berez, A., B.E. Peercy, and M. Starz-Gaiano. 2020. Development and analysis of a quantitative mathematical model of bistability in the cross repression system between APT and SLBO within the JAK/STAT signaling pathway. *Front. Physiol.* 11:803. https://doi.org/10.3389/fphys.2020.00803

Borensztejn, A., E. Boissoneau, G. Fernandez, F. Agnès, and A.-M. Pret. 2013. JAK/STAT autocontrol of ligand-producing cell number through apoptosis. *Development*. 140:195–204. https://doi.org/10.1242/dev.079046

Cai, D., S.-C. Chen, M. Prasad, L. He, X. Wang, V. Choesmel-Cadamuro, J.K. Sawyer, G. Danuser, and D.J. Montell. 2014. Mechanical feedback through E-cadherin promotes direction sensing during collective cell migration. *Cell*. 157:1146–1159. https://doi.org/10.1016/j.cell.2014.03.045

Cecchetelli, A.D., J. Hugunin, H. Tannoury, and E.J. Cram. 2016. CACN-1 is required in the *Caenorhabditis elegans* somatic gonad for proper oocyte development. *Dev. Biol.* 414:58–71. https://doi.org/10.1016/j.ydbio.2016.03.028

Chabu, C., and C.Q. Doe. 2009. Twins/PP2A regulates aPKC to control neuroblast cell polarity and self-renewal. *Dev. Biol.* 330:399–405. https://doi.org/10.1016/j.ydbio.2009.04.014

Chen, J., A.-C. Sayadian, N. Lowe, H.E. Lovegrove, and D. St Johnston. 2018. An alternative mode of epithelial polarity in the Drosophila midgut. *PLoS Biol.* 16:e3000041. https://doi.org/10.1371/journal.pbio.3000041

Chen, Y., N. Kotian, G. Aranjuez, L. Chen, C.L. Messer, A. Burtscher, K. Sawant, D. Ramel, X. Wang, and J.A. McDonald. 2020. Protein phosphatase 1 activity controls a balance between collective and single cell modes of migration. *eLife*. 9:e52979. https://doi.org/10.7554/eLife.52979

Cheung, K.J., V. Padmanaban, V. Silvestri, K. Schipper, J.D. Cohen, A.N. Fairchild, M.A. Gorin, J.E. Verdone, K.J. Pienta, J.S. Bader, and A.J. Ewald. 2016. Polyclonal breast cancer metastases arise from collective

dissemination of keratin 14-expressing tumor cell clusters. *Proc. Natl. Acad. Sci. USA*. 113:E854–E863. https://doi.org/10.1073/pnas.1508541113

Combedazou, A., V. Choesmel-Cadamuro, G. Gay, J. Liu, L. Dupré, D. Ramel, and X. Wang. 2017. Myosin II governs collective cell migration behaviour downstream of guidance receptor signalling. *J. Cell Sci.* 130:97–103. https://doi.org/10.1242/jcs.179952

Cox, D.N., S.A. Seyfried, L.Y. Jan, and Y.N. Jan. 2001. Bazooka and atypical protein kinase C are required to regulate oocyte differentiation in the *Drosophila* ovary. *Proc. Natl. Acad. Sci. USA*. 98:14475–14480. https://doi.org/10.1073/pnas.261565198

Cram, E.J., H. Shang, and J.E. Schwarzbauer. 2006. A systematic RNA interference screen reveals a cell migration gene network in *C. elegans*. *J. Cell Sci.* 119:4811–4818. https://doi.org/10.1242/jcs.03274

Dai, W., X. Guo, Y. Cao, J.A. Mondo, J.P. Campanale, B.J. Montell, H. Burrous, S. Streichan, N. Gov, W.-J. Rappel, and D.J. Montell. 2020. Tissue topography steers migrating *Drosophila* border cells. *Science*. 370:987–990. https://doi.org/10.1126/science.aaz4741

David, D.J.V., A. Tishkina, and T.J.C. Harris. 2010. The PAR complex regulates pulsed actomyosin contractions during amnioserosa apical constriction in *Drosophila*. *Development*. 137:1645–1655. https://doi.org/10.1242/dev.044107

Doherty, M.F., G. Adelmant, A.D. Cecchetelli, J.A. Marto, and E.J. Cram. 2014. Proteomic analysis reveals CACN-1 is a component of the spliceosome in *Caenorhabditis elegans*. *G3 (Bethesda)*. 4:1555–1564. https://doi.org/10.1534/g3.114.012013

Dunlop, J., X. Morin, M. Corominas, F. Serras, and G. Tear. 2004. Glaikit is essential for the formation of epithelial polarity and neuronal development. *Curr. Biol.* 14:2039–2045. https://doi.org/10.1016/j.cub.2004.10.048

Fica, S.M., C. Oubridge, M.E. Wilkinson, A.J. Newman, and K. Nagai. 2019. A human postcatalytic spliceosome structure reveals essential roles of metazoan factors for exon ligation. *Science*. 363:710–714. https://doi.org/10.1126/science.aaw5569

Geisbrecht, E.R., and D.J. Montell. 2002. Myosin VI is required for E-cadherin-mediated border cell migration. *Nat. Cell Biol.* 4:616–620. https://doi.org/10.1038/ncb830

Geisbrecht, E.R., and D.J. Montell. 2004. A role for Drosophila IAP1-mediated caspase inhibition in Rac-dependent cell migration. *Cell*. 118:111–125. https://doi.org/10.1016/j.cell.2004.06.020

Goswami, S., E. Sahai, J.B. Wyckoff, M. Cammer, D. Cox, F.J. Pixley, E.R. Stanley, J.E. Segall, and J.S. Condeelis. 2005. Macrophages promote the invasion of breast carcinoma cells via a colony-stimulating factor-1/epidermal growth factor paracrine loop. *Cancer Res.* 65:5278–5283. https://doi.org/10.1158/0008-5472.CAN-04-1853

Harmansa, S., I. Alborelli, D. Bieli, E. Caussinus, and M. Affolter. 2017. A nanobody-based toolset to investigate the role of protein localization and dispersal in *Drosophila*. *eLife*. 6:e22549. https://doi.org/10.7554/eLife.22549

Hatan, M., V. Shinder, D. Israeli, F. Schnorrer, and T. Volk. 2011. The *Drosophila* blood brain barrier is maintained by GPCR-dependent dynamic actin structures. *J. Cell Biol.* 192:307–319. https://doi.org/10.1083/jcb.201007095

Jang, A.C.-C., Y.-C. Chang, J. Bai, and D. Montell. 2009. Border-cell migration requires integration of spatial and temporal signals by the BTB protein Abrupt. *Nat. Cell Biol.* 11:569–579. https://doi.org/10.1038/ncb1863

Kumichel, A., K. Kapp, and E. Knust. 2015. A conserved di-basic motif of *Drosophila* crumbs contributes to efficient ER export. *Traffic*. 16:604–616. https://doi.org/10.1111/tra.12273

Labernadie, A., T. Kato, A. Brugués, X. Serra-Picamal, S. Derzsi, E. Arwert, A. Weston, V. González-Tarragó, A. Elosegui-Artola, L. Albertazzi, et al. 2017. A mechanically active heterotypic E-cadherin/N-cadherin adhesion enables fibroblasts to drive cancer cell invasion. *Nat. Cell Biol.* 19:224–237. https://doi.org/10.1038/ncb3478

Letizia, A., S. Sotillos, S. Campuzano, and M. Llimargas. 2011. Regulated Crb accumulation controls apical constriction and invagination in *Drosophila* tracheal cells. *J. Cell Sci.* 124:240–251. https://doi.org/10.1242/jcs.073601

Lin, P.-H., L.H. Huang, and R. Steward. 2000. Cactin, a conserved protein that interacts with the *Drosophila* IκB protein Cactus and modulates its function. *Mech. Dev.* 94:57–65. https://doi.org/10.1016/S0925-4773(00)00314-2

Majumder, P., G. Aranjuez, J. Amick, and J.A. McDonald. 2012. Par-1 controls myosin-II activity through myosin phosphatase to regulate border cell migration. *Curr. Biol.* 22:363–372. https://doi.org/10.1016/j.cub.2012.01.037

Manning, L., J. Sheth, S. Bridges, A. Saadin, K. Odinammadu, D. Andrew, S. Spencer, D. Montell, and M. Starz-Gaiano. 2017. A hormonal cue promotes timely follicle cell migration by modulating transcription profiles. *Mech. Dev.* 148:56–68. https://doi.org/10.1016/j.mod.2017.06.003

Matera, A.G., and Z. Wang. 2014. A day in the life of the spliceosome. *Nat. Rev. Mol. Cell Biol.* 15:108–121. https://doi.org/10.1038/nrm3742

Miao, G., D. Godt, and D.J. Montell. 2020. Integration of migratory cells into a new site in vivo requires channel-independent functions of innexins on microtubules. *Dev. Cell*. 54:501–515.e9. https://doi.org/10.1016/j.devcel.2020.06.024

Mishra, A.K., J.A. Mondo, J.P. Campanale, and D.J. Montell. 2019. Coordination of protrusion dynamics within and between collectively migrating border cells by myosin II. *Mol. Biol. Cell*. 30:2490–2502. https://doi.org/10.1091/mbc.E19-02-0124

Monahan, A.J., and M. Starz-Gaiano. 2013. Socs36E attenuates STAT signaling to optimize motile cell specification in the *Drosophila* ovary. *Dev. Biol.* 379:152–166. https://doi.org/10.1016/j.ydbio.2013.03.022

Montell, D.J., P. Rorth, and A.C. Spradling. 1992. Slow border cells, a locus required for a developmentally regulated cell migration during oogenesis, encodes *Drosophila* CEBP. *Cell*. 71:51–62. https://doi.org/10.1016/0092-8674(92)90265-E

Montell, D.J., W.H. Yoon, and M. Starz-Gaiano. 2012. Group choreography: Mechanisms orchestrating the collective movement of border cells. *Nat. Rev. Mol. Cell Biol.* 13:631–645. https://doi.org/10.1038/nrm3433

Murphy, A.M., and D.J. Montell. 1996. Cell type-specific roles for Cdc42, rac, and RhoL in *Drosophila* oogenesis. *J. Cell Biol.* 133:617–630. https://doi.org/10.1083/jcb.133.3.617

Niewiadomska, P., D. Godt, and U. Tepass. 1999. DE-Cadherin is required for intercellular motility during *Drosophila* oogenesis. *J. Cell Biol.* 144:533–547. https://doi.org/10.1083/jcb.144.3.533

Piacentino, M.L., Y. Li, and M.E. Bronner. 2020. Epithelial-to-mesenchymal transition and different migration strategies as viewed from the neural crest. *Curr. Opin. Cell Biol.* 66:43–50. https://doi.org/10.1016/j.ceb.2020.05.001

Pinheiro, E.M., and D.J. Montell. 2004. Requirement for Par-6 and Bazooka in *Drosophila* border cell migration. *Development*. 131:5243–5251. https://doi.org/10.1242/dev.01412

Ramel, D., X. Wang, C. Laflamme, D.J. Montell, and G. Emery. 2013. Rab11 regulates cell-cell communication during collective cell movements. *Nat. Cell Biol.* 15:317–324. https://doi.org/10.1038/ncb2681

Sauka-Spengler, T., and M. Bronner-Fraser. 2008. A gene regulatory network orchestrates neural crest formation. *Nat. Rev. Mol. Cell Biol.* 9:557–568. https://doi.org/10.1038/nrm2428

Savant-Bhonsale, S., and D.J. Montell. 1993. torso-like encodes the localized determinant of *Drosophila* terminal pattern formation. *Genes Dev.* 7:2548–2555. https://doi.org/10.1101/gad.7.12b.2548

Scarpa, E., and R. Mayor. 2016. Collective cell migration in development. *J. Cell Biol.* 212:143–155. https://doi.org/10.1083/jcb.201508047

Silver, D.L., E.R. Geisbrecht, and D.J. Montell. 2005. Requirement for JAK/STAT signaling throughout border cell migration in *Drosophila*. *Development*. 132:3483–3492. https://doi.org/10.1242/dev.01910

Silver, D.L., and D.J. Montell. 2001. Paracrine signaling through the JAK/STAT pathway activates invasive behavior of ovarian epithelial cells in *Drosophila*. *Cell*. 107:831–841. https://doi.org/10.1016/s0092-8674(01)00607-9

Starz-Gaiano, M., M. Melani, X. Wang, H. Meinhardt, and D.J. Montell. 2008. Feedback inhibition of Jak/STAT signaling by apontic is required to limit an invasive cell population. *Dev. Cell*. 14:726–738. https://doi.org/10.1016/j.devcel.2008.03.005

Stuelten, C.H., C.A. Parent, and D.J. Montell. 2018. Cell motility in cancer invasion and metastasis: Insights from simple model organisms. *Nat. Rev. Cancer*. 18:296–312. https://doi.org/10.1038/nrc.2018.15

Tannoury, H., V. Rodriguez, I. Kovacevic, M. Ibourk, M. Lee, and E.J. Cram. 2010. CACN-1/Cactin interacts genetically with MIG-2 GTPase signaling to control distal tip cell migration in *C. elegans*. *Dev. Biol.* 341:176–185. https://doi.org/10.1016/j.ydbio.2010.02.025

Thakran, P., P.A. Pandit, S. Datta, K.K. Kolathur, J.A. Pleiss, and S.K. Mishra. 2018. Sde2 is an intron-specific pre-mRNA splicing regulator activated by ubiquitin-like processing. *EMBO J.* 37:89–101. https://doi.org/10.15252/embj.201796751

Valanne, S., J.-H. Wang, and M. Rämet. 2011. The *Drosophila* Toll signaling pathway. *J. Immunol.* 186:649–656. https://doi.org/10.4049/jimmunol.1002302

Wang, H., Z. Qiu, Z. Xu, S.J. Chen, J. Luo, X. Wang, and J. Chen. 2018. aPKC is a key polarity determinant in coordinating the function of three distinct

cell polarities during collective migration. *Development*. 145:dev158444. https://doi.org/10.1242/dev.158444

Wang, X., J. Bo, T. Bridges, K.D. Dugan, T.-c. Pan, L.A. Chodosh, and D.J. Montell. 2006. Analysis of cell migration using whole-genome expression profiling of migratory cells in the *Drosophila* ovary. *Dev. Cell*. 10:483–495. https://doi.org/10.1016/j.devcel.2006.02.003

Wang, X., L. He, Y.I. Wu, K.M. Hahn, and D.J. Montell. 2010. Light-mediated activation reveals a key role for Rac in collective guidance of cell movement in vivo. *Nat. Cell Biol.* 12:591–597. https://doi.org/10.1038/ncb2061

Xu, S., S. Tyagi, and P. Schedl. 2014. Spermatid cyst polarization in *Drosophila* depends upon apkc and the CPEB family translational regulator orb2. *PLoS Genet.* 10:e1004380. https://doi.org/10.1371/journal.pgen.1004380

Yang, J., P. Antin, G. Berx, C. Blanpain, T. Brabletz, M. Bronner, K. Campbell, A. Cano, J. Casanova, G. Christofori, et al. 2020. Guidelines and definitions for research on epithelial-mesenchymal transition. *Nat. Rev. Mol. Cell Biol.* 21:341–352. https://doi.org/10.1038/s41580-020-0237-9

Zanini, I.M.Y., C. Soneson, L.E. Lorenzi, and C.M. Azzalin. 2017. Human cactin interacts with DHX8 and SRRM2 to assure efficient pre-mRNA splicing and sister chromatid cohesion. *J. Cell Sci.* 130:767–778. https://doi.org/10.1242/jcs.194068

Supplemental material

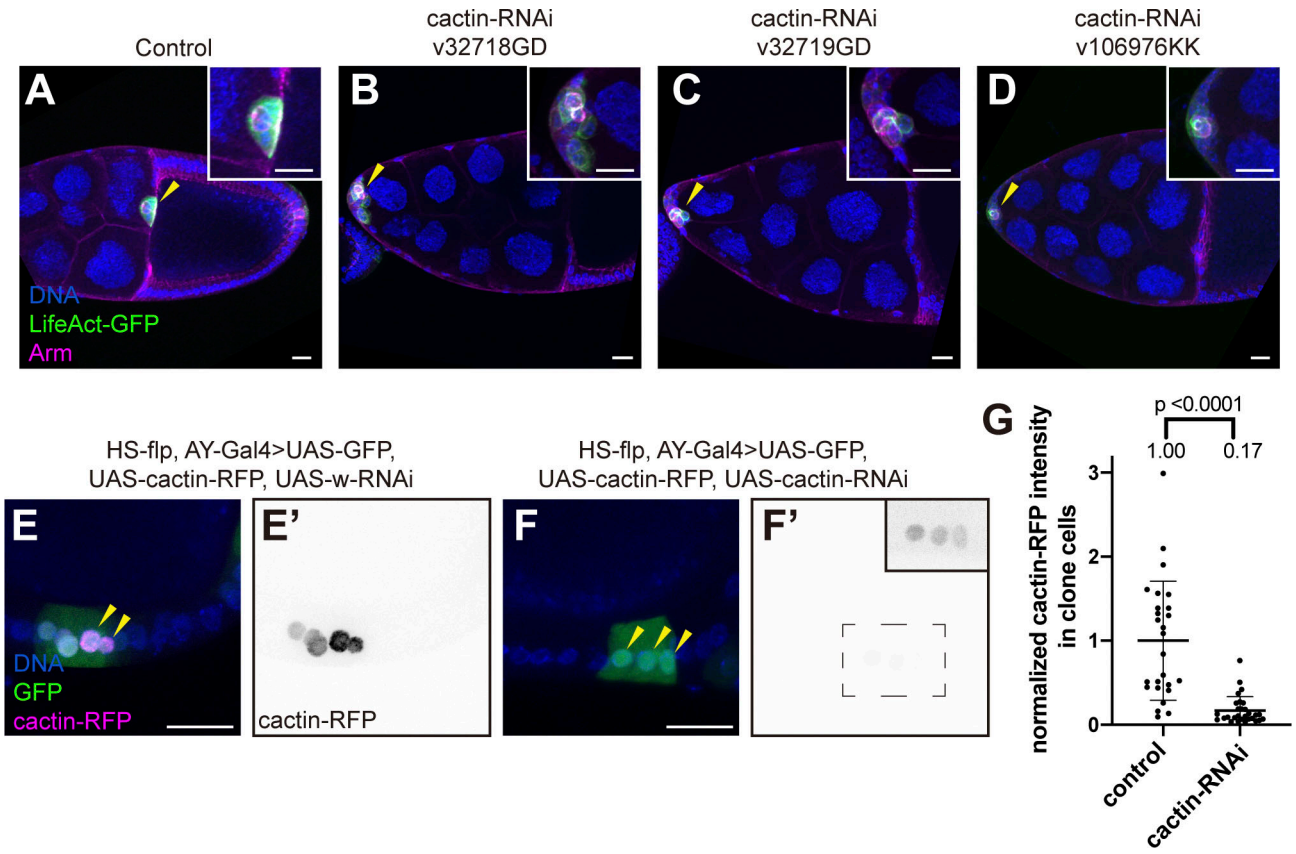

Figure S1. **Multiple *cactin*-RNAi lines cause delamination defects.** Related to Fig. 1. **(A–D)** Confocal images of stage 10 egg chambers with c306-Gal4 driving UAS-LifeAct-GFP together with (A) control (crossed to *w1118*), (B) UAS-*cactin*-RNAi (v32718GD), (C) UAS-*cactin*-RNAi (v32719GD), or (D) UAS-*cactin*-RNAi (v106976KK). Insets show high magnification of border cell clusters. Yellow arrowheads indicate the border cell cluster position. **(E and F)** HS-flp-out clones showing UAS-*cactin*-RNAi efficiency in follicle cells. GFP (green) labels Gal4-expressing clones. Hoechst DNA dye is in blue. Cactin::RFP is in magenta. **(E)** Image of UAS-*cactin*::RFP with UAS-*w*-RNAi. **(F)** Image of UAS-*cactin*::RFP with UAS-*cactin*-RNAi. Yellow arrowheads indicate the Cactin-RFP expression in clones. **(E′ and F′)** Cactin-RFP single channel in E and F. **(F′)** Imaging settings were the same for E′ and F′, whereas the inset in F′ shows enhanced contrast to reveal the low level of remaining Cactin-RFP expression. Scale bars, 20 µm. **(G)** Quantification of Cactin-RFP intensity in HS-flp-out clone cells. The mean of control (*w*-RNAi) is normalized to 1. Each dot represents a cell.

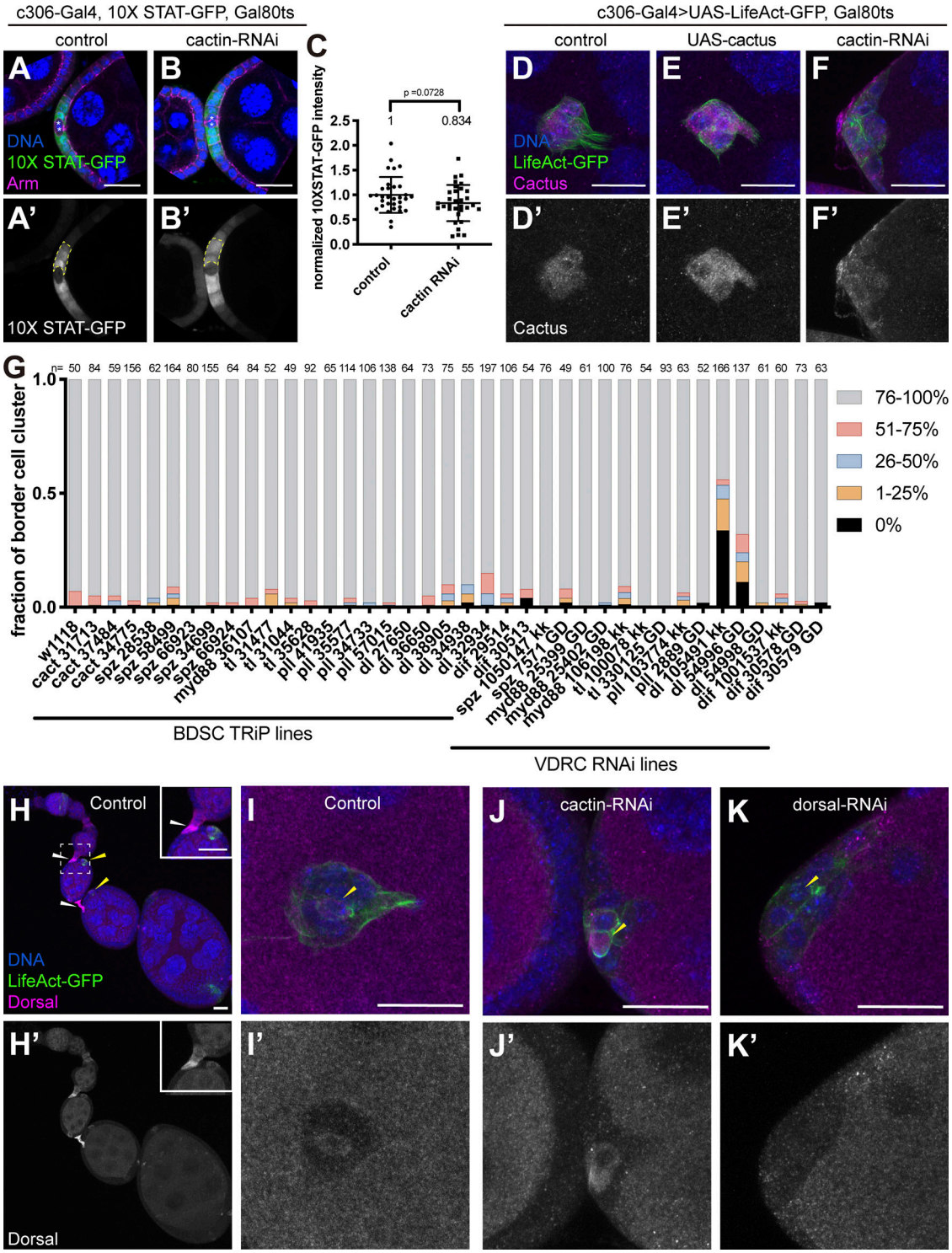

Figure S2. **Cactin functions independently of JAK/STAT or Toll signaling pathways in border cells.** Related to Fig. 1. **(A and B)** Images of stage 8 egg chambers of c306-Gal4, ubi-Gal80ts combined with 10×STAT-GFP together with (A) control (crossed to *w1118*) or (B) UAS-*cactin*-RNAi. White asterisks mark the polar cells. **(A′ and B′)** 10×STAT-GFP single channel. The yellow dashed lines mark the follicle cells next to the polar cells. **(C)** Quantification of the 10× STAT-GFP intensity in marked follicle cells. Each dot represents an egg chamber. **(D–F)** Images of anti-Cactus staining with c306-Gal4 driving UAS-LifeAct-GFP together with (D) control (crossed to *w1118*), (E) UAS-*cactus*, or (F) UAS-*cactin*-RNAi. **(D′–F′)** Images show the anti-Cactus single channel. **(G)** Quantification of delamination defects in stage 10 egg chambers with UAS-RNAi lines of Toll signaling components. **(H–K)** Images of anti-Dorsal staining with c306-Gal4 driving UAS-LifeAct-GFP together with (H) control (crossed to *w1118*) early stages, (I) control (crossed to *w1118*) stage 9, (J) UAS-*cactin*-RNAi, stage 9, or (K) UAS-*dorsal*-RNAi, stage 9. **(H′–K′)** Images show the anti-Dorsal single channel. **(H)** Inset shows the high magnification image of the stalk. White arrowheads indicate the stalks. Yellow arrowheads indicate the polar cells. Scale bars, 20 µm.

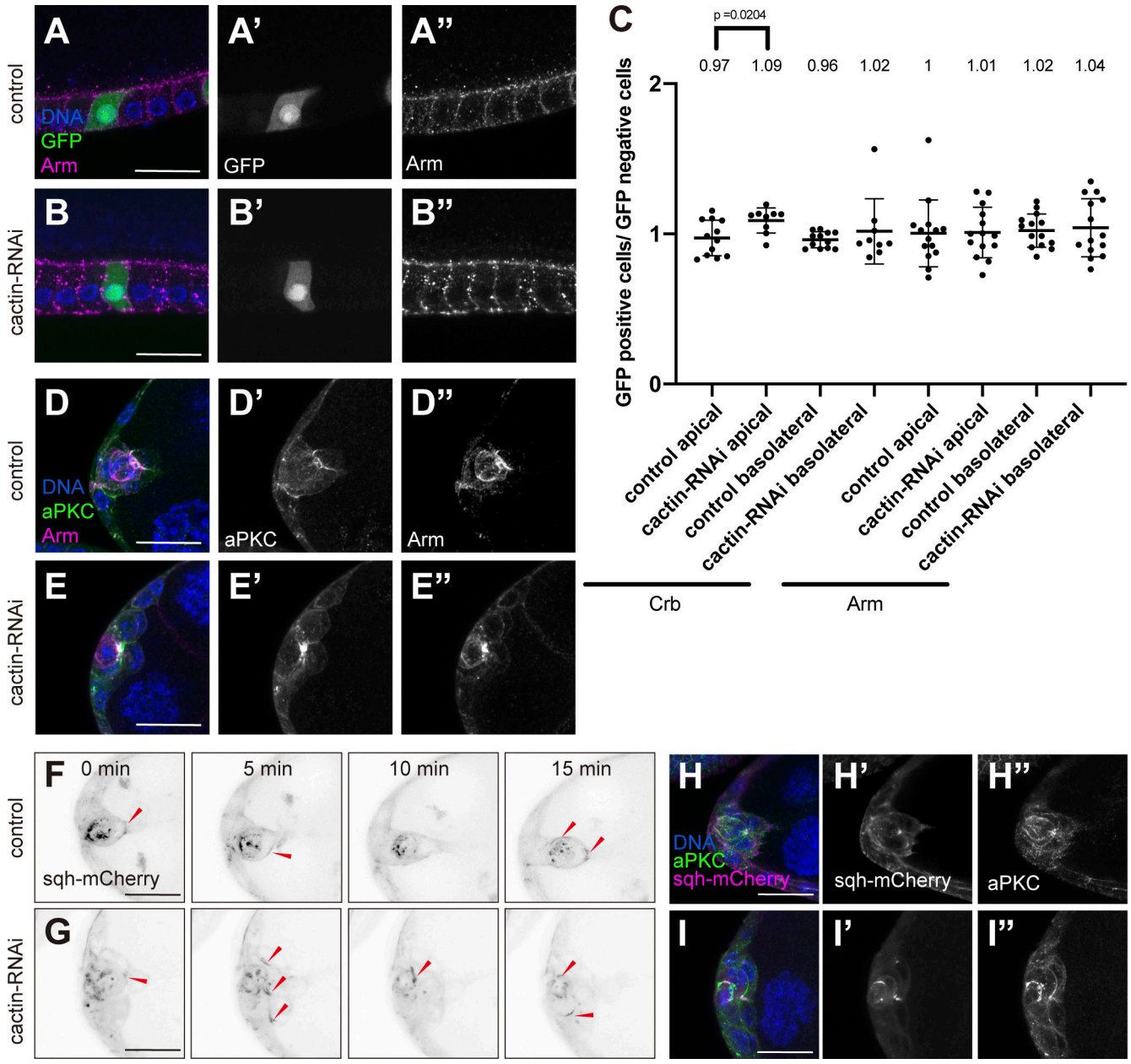

Figure S3. **Excess apical Crb in Cactin knockdown cells.** Related to Fig. 3. **(A–B″)** HS-flp-out clones showing anti-Arm staining in follicle cells. **(A–A″)** Control (UAS-*w*-RNAi). **(B–B″)** UAS-*cactin*-RNAi. **(A′, A″, B′, and B″)** Images show the single channels in A and B. **(C)** Quantification of Crb and Arm staining intensity in HS-flp-out clones. The ratio of Crb and Arm staining intensity in RNAi clones (GFP+ cells)/non-RNAi clones (GFP− cells) is shown. **(D–E″)** Images of anti-aPKC and anti-Arm co-staining border cell clusters with c306-Gal4 together with (D) control (cross to *w1118*) or (E) UAS-*cactin*-RNAi. **(D′, D″, E′, and E″)** Images show the single channels of aPKC and Arm in D and E. **(F and G)** Snapshots of time-lapse videos of c306-Gal4 combined with sqh-mCherry together with (F) control (cross to *w1118*) or (G) UAS-*cactin*-RNAi. Red arrowheads indicate the dynamic localization of sqh-mCherry during the delamination process. **(H–I″)** Images of anti-aPKC and anti-mCherry co-staining border cell clusters with c306-Gal4 combined with sqh-mCherry together with (H) control (cross to *w1118*) or (I) UAS-*cactin*-RNAi. **(H′, H″, I′, and I″)** Images show the single channels of aPKC and sqh-mCherry in H and I. Scale bars, 20 µm.

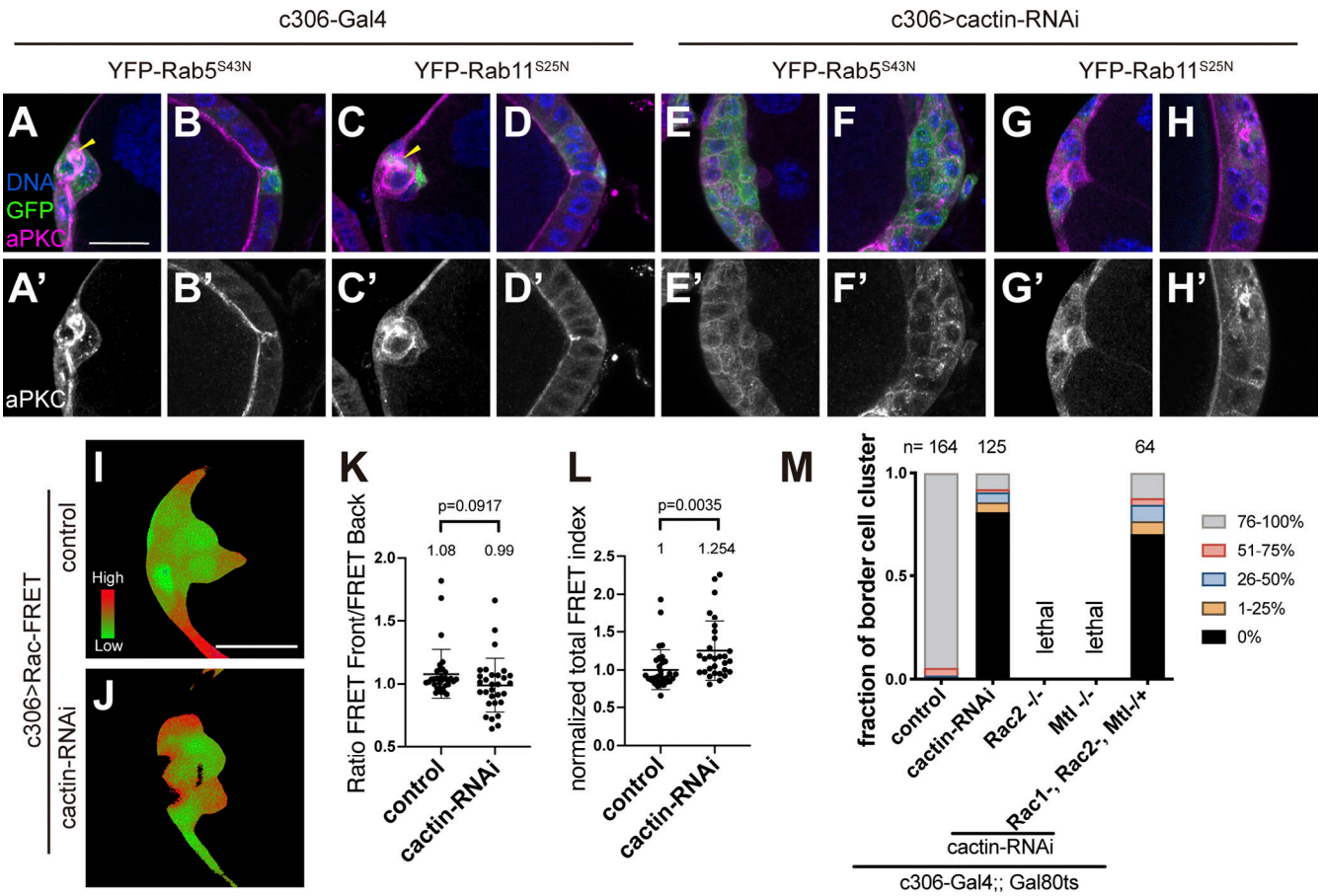

Figure S4. ***cactin*-RNAi indirectly affects Rac activity in border cells.** Related to Fig. 4. **(A–D)** Images of anti-aPKC staining egg chambers of c306-Gal4 together with (A and B) UAS-YFP-Rab5^{S43N} or (C and D) UAS-YFP-Rab11^{S25N}. **(A and C)** Images of border cell clusters. Yellow arrowheads indicate the apical junctions in the border cell clusters. **(B and D)** Images of posterior follicle cells. **(A′–D′)** Images show the single channel of anti-aPKC in A–D. **(E–H)** Images of anti-aPKC staining egg chambers of c306-Gal4 driven UAS-*cactin*-RNAi together with (E and F) UAS-YFP-Rab5^{S43N} or (G and H) UAS-YFP-Rab11^{S25N}. **(E and G)** Images of border cell clusters. **(F and H)** Images of posterior follicle cells. **(E′–H′)** Images show the single channel of anti-aPKC in E–H. **(I and J)** FRET images of border cell clusters of c306-Gal4 driven UAS-Rac-FRET together with (I) control (cross to *w1118*) or (J) UAS-*cactin*-RNAi. Scale bars, 20 µm. **(K)** Quantification of Front/Back FRET ratio in Control and cactin-RNAi. Each dot indicates a border cell cluster. **(L)** Quantification of the total FRET index in the border cell cluster. Each dot indicates a border cell cluster. **(M)** Quantification of delamination defects in stage 10 egg chambers.

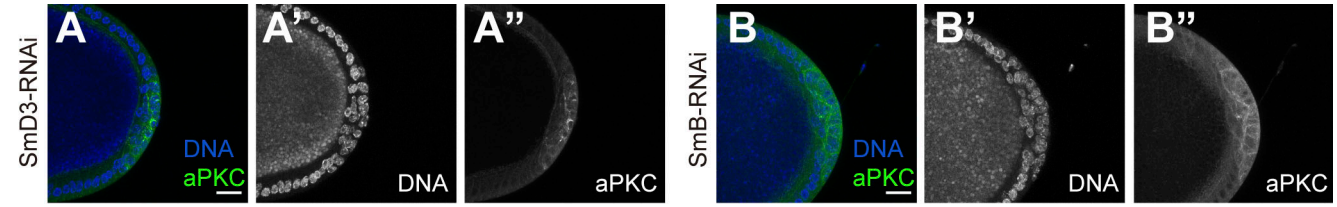

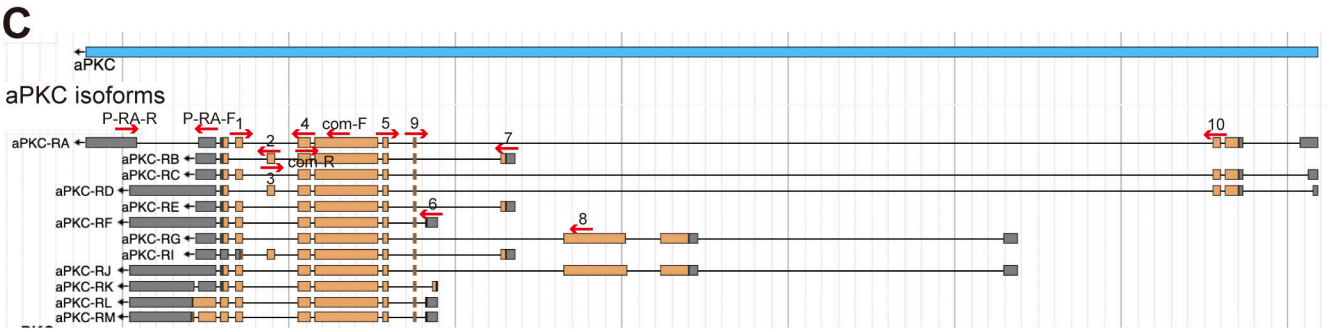

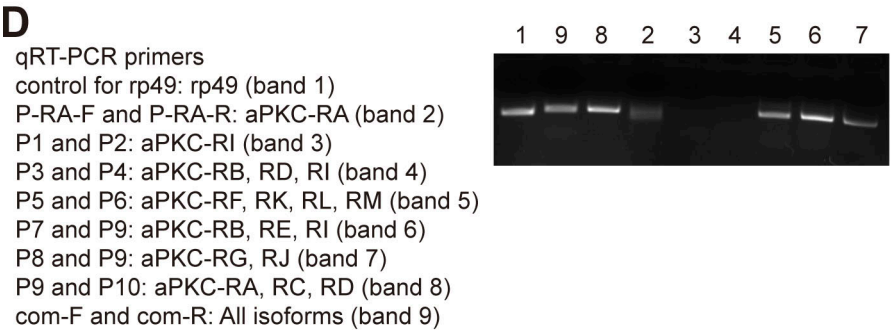

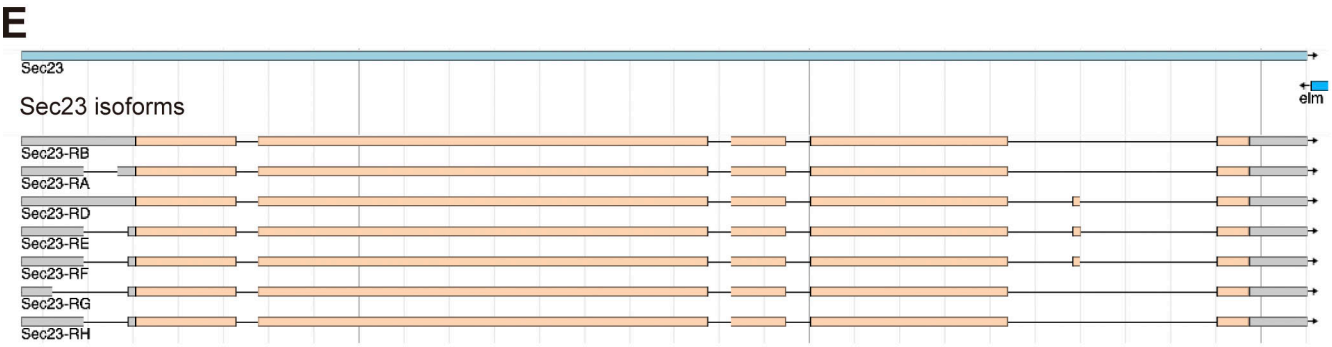

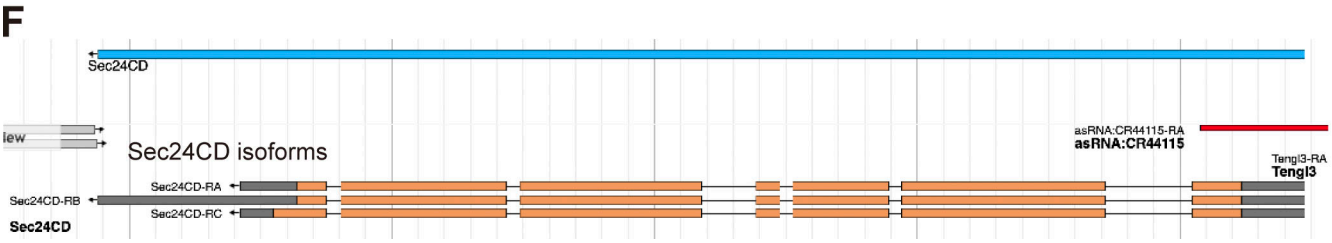

Figure S5. **Cactin regulates aPKC and Crb localizations via its spliceosome function.** Related to Figs. 5 and 6. **(A–B″)** Images of anti-aPKC staining of the posterior follicle cells with c306-Gal4 together with (A–A″) UAS-*SmD3*-RNAi or (B–B″) UAS-*SmB*-RNAi. **(A′ and B′)** DNA single channel. **(A″ and B″)** aPKC single channel. Scale bars, 20 µm. **(C)** Schematic of aPKC isoforms and primers designs for qRT-PCR. Orange rectangles represent the protein coding regions in exons. Gray rectangles represent the UTR regions in exons. Black lines between orange and gray rectangles represent introns. Red arrows represent the primers designed for qRT-PCR. **(D)** Gel electrophoresis image showing RT-PCR results of aPKC isoforms. **(E)** Schematic of Sec23 isoforms. **(F)** Schematic of Sec24CD isoforms. Note that C, E, and F are snapshots from the flybase website (https://www.flybase.org). Source data are available for this figure: SourceData FS5.

Video 1. **Time-lapse videos of the border cell delamination process in control and cactin knockdown clusters.** LifeAct-GFP expression is driven by c306-Gal4 to label the border cell cluster in white. Time-lapse imaging was performed using a 40 × 1.4 NA water immersion objective by Zeiss 800 confocal microscope. 1-µm-thick z-sections including the entire border cell cluster were collected for 101 min at 1-min intervals. The video is played at 7 frames/s. Egg chamber genotype: c306-Gal4>UAS-LifeAct-GFP/+ (control, left) and c306-Gal4>UAS-LifeAct-GFP, UAS-*cactin*-RNAi (right). Related to Fig. 2.

Video 2. **Time-lapse videos of Myosin-II dynamics during the delamination process.** The Myosin-II light chain tagged with mCherry (Sqh::mCherry) is shown in black. Time-lapse imaging was performed using a 40 × 1.4 NA water immersion objective by Zeiss 800 confocal microscope. The 1-µm-thick z-sections including the entire border cell cluster were collected for 21 min at 1-min intervals. The video is played at 5 frames/s. Egg chamber genotypes: c306-Gal4, sqh-mCherry/+ (control, left) and c306-Gal4>UAS-*cactin*-RNAi/sqh-mCherry (right). Related to Fig. S3.

Provided online are two tables. Table S1 shows the 289 genes whose isoform proportions changed significantly in *cactin*-RNAi. Table S2 shows the gene ontology and pathway analyses of the 289 genes.